Reply to the reviewers for the second review of Gregor et al: Interannual drivers of the seasonal cycle of CO2 in the Southern Ocean

We would like to thank the reviewers for their thorough reviews of the paper and we appreciate the time taken to hone the manuscript towards publication. We have made relatively large changes to the manuscript with changes to both figures and text. In particular we have addressed the issue of uncertainty a lot more thoroughly. This means that the content of section 3.5 (winter) has changed a fair deal. In addition we have also made use of a professional editor, which has hopefully reduced the amount of editorial mistakes in the manuscript to an acceptable amount.

Below we address the comments of the reviewers in blue. After that we show the track changes for the document.

2nd review of Gregor et al: Interannual drivers of the seasonal cycle of CO2 in the Southern Ocean

Response to previous concerns:

Previously, I have raised 3 main concerns. The first related to the very confusing presentation of variability and trends, the second related to the missing evaluation of uncertainties (of various sources) and the third related to the choice of time periods as they are compared in the text.

In their revised manuscript, the authors have indeed taken into consideration the concerns raised by this reviewer, however, as I will outline below, they still miss to clearly communicate the uncertainty of their analysis and thereby still present results overconfidently.

Firstly though, the authors have done a good job in their manuscript to clarify when they consider trends and variability and what is the time period considered. This makes the manuscript much easier to read. Exceptions however still exist, e.g. the abstract line 21 (here authors talk about "interannual trends") and on page 21 line 70, where the authors state "… summer drivers may explain the inter-annual variability in the decadal trends". These statements need clarification – see my previous review.
We have changed the wording to avoid the confusing the decadal trends (with this short time-series); however, in the first part of the paragraph on page 21, we refer to the decadal trends in the cited publications, which do consider longer time series from which decadal variability can be derived.

Coming back to the uncertainty analysis: The authors now provide an error assessment which is a great leap forward, however, when discussing the results the new uncertainty estimates are often mentioned but likewise not properly taken into consideration. To give you a concrete example: Uncertainties are still only hand-wavy included in figure 4 which makes me doubt that these observed short temporal variabilities are real or just statistical noise given that these fluctuations are often in the order of 2-3 µatm (visually assessment based on figure 4). Figure 2 likewise suggests errors beyond the displayed differences between methods. Another example is figures 5 and 6. Here the authors do add the uncertainty, but fail to properly discuss the limitation that basically the majority of the SO variability is insignificant, besides a few regions. Instead the authors assume the significant regional drivers are representative for the entire region. The authors further only mention uncertainty in a first sentence of the sections but then it is not clear if this is properly taken into consideration when discussing the drivers (see specific comments below).
We have changed figure 4 to now show the uncertainty surrounding ensemble estimates for summer and winter. We feel that this is now far more explicit around the error. Moreover, we realise that the interannual variability is

Regarding my third point, the authors still don't make a strong enough case for their periods they consider. They refer in the text to figure 4 but visually it is not obvious why the periods have been chosen. I am aware that this is a new argument (as I have previously only criticized the length of the periods). This however can be easily solved by adding a sentence or 2 explaining why these periods were chosen (may this be due to some metric or subjective choice)
We have changed the motivation for our time periods slightly. We also add a sentence at the

end of the paragraph that makes it clear that we do not feel that our study is dependent on these specific period lengths or starting years: *"In order to capture the decoupled 4–6 year short-term variability observed in summer, the estimates are divided into four objectively selected periods (P1 to P4). The periods are each four years long with the exception of P1, which is five years long due to the fact that the time-series is not divisible by four (with a length of 17 years in total). Given a longer time series, this analysis would benefit from testing different lengths for each period, as well as varying the starting and end years."*

In summary, I think the manuscript has improved, but overall, issues remain regarding the uncertainty of the analysis. This really pains me because I do think that the paper is important and I do very much like the approach based on looking at anomalous periods (rather than linear trends). Also, an assessment based on 2 novel methods is a welcome addition to assessment papers such as the recently published Ritter et al. (GRL) Southern Ocean SOCOM trend comparison. I don't think that (many of) the conclusions drawn would fall based on the error assessment, but in a data sparse region like the Southern Ocean, where all methods rely on heavy data extrapolation the uncertainty must be on the forefront of any variability, trend or process study.

Recommendation:

Based on the revision, I cannot recommend the manuscript for publication. Instead I would like to see a revised manuscript, where the authors really discuss their results in in a fair way in light of the uncertainty they are facing. Plus I suggest the authors check remaining editorial issues. I am convinced that after this step (plus some minor comments below) the paper can become acceptable for publication in BG.

Specific comments:

In general: Many editorial issues need to be fixed. E.g. in many instances commas are missing, the authors switch between present tense and past tense (e.g. in the abstract) and figure 7 is labelled figure 9. I will not list them all here, but rather suggest professional text editing.
We have sent the document to a professional editor and we hope that the mistakes have now been reduced to an acceptable amount.

Abstract line 9-10: (a) very minor but SOCAT includes fCO_2 not pCO_2 and (b) "… ship measurements of pCO_2 (SOCAT) …" really is a clumsy way to introduce SOCAT. Firstly, the abbreviation SOCAT needs to be defined (Surface Ocean CO2 Atlas) and secondly, what about LDEO? This database equally includes pCO_2 ship measurements.
We leave the introduction of SOCAT to the methods section of the manuscript.

Abstract line 13: "… nine regions defined by basin …" – at this time you have not mentioned the Southern Ocean so the reader gets the impression you talk about the actual basins.
We have made this more clear; however, it should be clear from the title that we consider the Southern Ocean in this study.

Abstract line 15: delta pCO_2 is not defined (i.e that you mean the difference between ocean and atmosphere – it may as well be the seasonal difference).
Changed to accommodate the seasonal differences

Abstract line 21: “Interannual trends” - see my previous assessment
This has been addressed: we refer now only to interannual variability.

Abstract line 22: “… chlorophyll-a variability where the latter had high mean seasonal concentrations.” It is not clear what the authors try to say here
We have tried to clarify this: where higher concentrations of chlorophyll-*a* correspond with lower $p\mathrm{CO_2}$ concentrations.

Introduction line 32: “accurately measure” – I suggest “accurately quantify”. Measurements of any quantity have reached high accuracy. The interpretation through interpolation methods (such as this study – hence the necessity of an uncertainty estimate) suffer from lower accuracy.
Changed as suggested

Introduction lines 34 and 35: “Empirical models provide an interim solution to this challenge until prognostic ocean biogeochemical models are able to represent the Southern Ocean CO2 seasonal 35 cycle accurately“ – it is not clear from the context of the text why the seasonality is suddenly important here
Have made this a little more general for the first paragraph, we then later address the importance of the seasonal cycle later in the introduction.

Introduction line 37: “source in the 1990’s” – I am not aware of any study that suggests the Southern Ocean was a source in the 1990’s. Studies of Le Quéré and Lovenduski only suggest a saturation of the sink. Do you refer to a specific region or a specific season or both?
Changed to weakening sink / strengthening sink

Introduction line 44: Not all proxies in the literature are satellite proxies.
Have changed this: *The proxies are often satellite observable, but may include climatologies or output from assimilative models.*

Introduction line 47: The Landschutzer et al 2015 paper focuses on 2002-2011 and not 2000-2010
Changed accordingly

Introduction line 56-57: Additionally, the Xue et al 2015 paper suggests the same trends based on observations south of Tasmania and should be cited.
Included the Xue et al. (2015) study: *This is supported by observations from the Drake Passage and south of Australia showing that variability of upwelling has affected* $\Delta\, p\mathrm{CO_2}$ *(Munro et al., 2015; Xue et al., 2015).* We discuss the role of the SAM in driving this variability in the following paragraph, where Xue et al. (2015) is cited again.

Page 3 line 92: It is “Self-Organizing Map” – i.e. singular not plural.
Corrected

Page 4 line 2: “v2.2” This is not the SOM-FFN version the authors refer to, but the version of the database where the data are stored.
Changed this identifier to the run id: netG05

Results: See also main comments above.

Page 4 line 18: "comparing the different products is beyond the scope of this study" is a clumsy formulation. The authors do compare products here, but pCO2. The phrase should rather read that comparing proxies is beyond the scope of this study
… comparing the different proxies used in each of the CO_2 products is beyond the scope of this study.

Page 6 line 73: The first sentence is not necessary – of course you discuss the results in the results section
Sentence removed

Figures 2 and 4: Add uncertainty alongside the lines. Not as numbers. It is difficult to compare lines with numbers. At the moment, it looks like the authors try and highlight a difference between methods in Figure 2 that is not statistically significant (given the Ew and Eb numbers) as well as amplitude anomalies (green and blue) in Figure 4 that are as well not significant based on the Eb. This is very confusing. So, my question to the authors is: Can you actually say – with absolute certainty – that (a) any of the 3 methods is at any given point in time statistically significantly different from any of the other methods? (b) That anomalies are – with absolute certainty - the result of environmental conditions and not simply the result of internal variability? Based on the evidence presented, I doubt you can.
We are now far more cautious about our results. We also show the uncertainties in Figure 4. Figure 5 is dedicated to showing the regional errors (moved from the supplementary materials), and we also show uncertainty in the plots for the drivers (Figures 6 and 7). Addressing now the specific points: (a) we agree that the methods are likely not statistically significant at any given time; however we do feel that it is necessary to explain the observed differences as they contribute to the between method error. (b) We are a bit more cautious with ascribing the drivers to changes in ΔpCO2 and describe the changes only where the between method uncertainty is acceptable.

Page 8 line 10: The authors missed my point in the first review round. I have noted that I have not seen any evidence that the CLUSTERING step is causing the difference. I am well aware that there is a difference and I do trust the authors with their assessment that the difference comes from the SOM method, but in neither of the papers I have seen any evidence that it is in fact the CLUSTERING step responsible for the mismatch. Many people are using the Landschutzer product, hence such an assessment of the cluster-based mismatch would be very valuable to the community. So, in summary: it is not enough to point at a difference plot and jumping to mechanistic conclusions. The authors should rather add a more in-depth analysis – also comparing the products to actual observations - if they want to add such a conclusive statement.
We've removed the statement that clustering is the driver of this difference, but may look into this in a bit more detail in a later study.

Page 9 line 21: Is the MIZ now in- or excluded? Later on, it is mentioned again. And if it is excluded, then why mention it at all?
Have removed panel c from Figure 2 (MIZ) and masked in Figure 3. References to the MIZ in the remainder of the text have been removed.

Page 9 line 34: Figure 3 a-d
Corrected

Page 10 line 54: Now the MIZ is discussed again – very confusing
Removed this sentence

Page 10 line 65: Only 6 are shown? Why? Is the MIZ in or out? It seems that it is ignored in the figures but added to the text. This is misleading the reader.
We have removed the MIZ estimates from the main text – inconsistent coverage between methods, large errors (stemming from little data).

Page 11 line 88: "however, our confidence in the changing trend is low due to lack of coherence between methods (Figure 2a,b) and only three years of data, with little data in 2014." – This statement is a bit of a surprise. Here the authors highlight that their trends are uncertain, but in the following they discuss the short term IAV as if it only little uncertainty is present. In contrast, Rodenbeck et al 2015, Landschutzer et al 2015 and Ritter et al 2017 show that trends are more robust among methods than IAV. Please explain or expand.
We have now addressed the variability of IAV between methods more explicitly. We hope that this addresses the reviewers concerns. Moreover, we have removed this statement as we agree that it is conceptually inconsistent.

Page 13 line 35: "The 335 mean of the method anomalies for each transition is then taken. These anomalies are considered significant if the absolute estimate of the anomaly is larger than the standard deviation between the methods for each period" – all fine, but I am puzzled why one uncertainty estimate is in the methods section and the other is in the appendix?
The section in the supplementary materials about the calculation of uncertainty in Figures 6 and 7 has been moved to the main text.

Page 13 line 47: The authors here mention that the uncertainty estimate masks out large regions. They equally and rightfully point out that there are other regions that are not masked and that those are considered. I do agree with the author's driver assessment in the following but now my question: Based on the assessment of the fewer, significant regions, how much can one assume that the driver assessment is also driving the variability of the larger – insignificant SO. I don't think one can with absolute certainty.
Plotted the uncertainty mask on the driver anomalies too. We have adjusted the text accordingly – this has led to substation changes in Section 3.5.

Page 15 line 99: "However, seasonal – regional analysis shows that the observed relationship between pCO2 and SST is counterintuitive (Figure 5a-c,g-i). On this basis we propose that SST is not a driver of pCO2 in winter." – Hold on here: Firstly, this is not a new proposal but has been e.g. shown by Takahashi et al 2002. Secondly, despite temperature not being the driver, the solubility relation still exists, it is simply not dominating the variability (see e.g. Figure 3 of Landschutzer 2015). Thirdly, 2-3 lines earlier the authors mention that they propose changes in wind stress as an alternative hypothesis to Landschutzer 2015, but this is exactly the point of the Landschutzer paper, that changes in the wind pattern and thereby changes in wind stress and upwelling caused the reinvigoration of the SO sink (see again e.g. Figure 3 in Landschutzer et al). The main difference is that these authors have not done the analysis for winter separately.
We have changed this paragraph accordingly to state that the finding is a refinement of the hypothesis put forward by Landschützer et al. (2015) in that we add a seasonal constraint.

Page 16 lines 28 onward: The authors talk about correlations, but based on the visual comparison it is not easy to verify this assessment. It would help to add an actual correlation plot, or adjust the colour scheme.
We have added the correlations for each driver anomaly with $\Delta pCO2$ anomalies on the respective driver. This has been done for Figures 6 and 7

Page 16 line 35: "Looking more specifically at the significant variability…" – Now I am completely lost. Do the authors now, as they state in the beginning, only consider significant regions or not? This statement suggests that they did not but start doing so now.
This is has been removed to avoid this confusion.

Suggestions for revision or reasons for rejection (will be published if the paper is accepted for final publication)

Reference for Interannual driver of the seasonal cycle of CO2 fluxes in the Southern Ocean
Luke Gregor, Schalk Kok, and Pedro M. S. Monteiro

This paper is much improved and I thank the authors for considering each of the concerns and recommendations of the first-round reviewers. I think with some minor revisions, this paper will be ready for publication and an excellent contribution to the field. Below are a few comments and suggestions. Also, the included line numbers seem to not extend past 100 before starting again from 00 so I include page and line numbers in order to help locate my references.

I think that Figure 2 is very clear to help the reader visualize the products described here. Figure 2d is specifically interesting. However, it should be considered that the amount of area covered by the summer MIZ region is different from the winter MIZ region. When calculating the standard deviation you need to account for that.
We have removed the references to the MIZ at the recommendation of Reviewer 1. We show the plots of the MIZ in the Supplementary materials.

Figure 3: The ice mask varies by season in this figure but I don't understand what the source of the mask is. The SOM-FFN product specifically has the same coverage through all seasons I know. Is the mask just the regions where all 3 ensemble members have values for that season? I could see that the chosen MLD or Chl product input could limit this coverage during certain seasons, but just making it clear where that comes from would be helpful. Also, you could consider not showing the MIZ region all together since you state on Page 9, in line 21 that you are excluding it from the paper.
We have adopted the recommendation, masking the MIZ for Figure 3.

Throughout the manuscript, I strongly suggest you take care when using the word "data" to describe the output form these machine learning methods. Someone not as familiar with the topic could be led to believe we actually have observations everywhere that you show (for example on Page 11, line 84).
We have changed data (referring to interpolated data) to estimates.

Lastly, in the synthesis, it should be noted that this shorter timeframe could bias/limit the results presented here and only with increased timeseries of not only pCO2 but also these drivers (and the need for continued sustained satellite observations) will this work be validated and improved upon.
We have added this statement to the summary.

Interannual drivers of the seasonal cycle of CO_2 in the Southern Ocean

Luke Gregor[1,2], Schalk Kok[3] and Pedro M. S. Monteiro[1]

[1] Southern Ocean Carbon-Climate Observatory (SOCCO), CSIR, Cape Town, South Africa
[2] University of Cape Town, Department of Oceanography, Cape Town, South Africa
[3] University of Pretoria, Department of Mechanical and Aeronautical Engineering, Pretoria, South Africa

Correspondence to: Luke Gregor (luke.gregor@uct.ac.za)

Abstract.

Resolving and understanding the drivers of variability of CO_2 in the Southern Ocean and its potential climate feedback is one of the major scientific challenges of the ocean-climate community. Here we use a regional approach on empirical estimates of pCO_2 to understand the role that seasonal variability has on long term CO_2 changes in the Southern Ocean. Machine learning has become ~~a useful~~the preferred empirical modelling tool to interpolate time- and location-restricted ship measurements of pCO_2 ~~(SOCAT) to a gridded map using satellite data.~~. In this study we use an ensemble of three machine~~-~~-learning ~~methods~~products: Support Vector Regression (SVR) and Random Forest Regression (RFR) from Gregor et al. (2017~~);~~), and the SOM-FFN method from Landschützer et al. (2016). The interpolated ~~data were~~estimates of ΔpCO_2 are separated into nine regions in the Southern Ocean defined by basin (Indian, Pacific and Atlantic) and biomes (as defined by Fay and McKinley, 2014a). The regional approach ~~showed a meridional gradient and zonal asymmetry in the magnitude of ΔpCO_2 estimates. Importantly, there was a~~shows that, while there is good agreement in the overall trend of the products, there are periods and regions where the confidence in estimated ΔpCO_2 is low due to disagreement between the products. The regional breakdown of the data highlighted the seasonal decoupling of the modes for summer and winter interannual variability. Winter interannual variability had a longer mode of variability compared to summer, which varied on a 4–6 year time scale. ~~To understand this variability of ΔpCO_2, we investigated changes in summer and winter ΔpCO_2 and the drivers thereof. The dominant winter changes are driven by wind stress variability. This is consistent with the temporal and spatial characteristics of the Southern Annular Mode (SAM), which has a decadal mode of variability (Lovenduski et al., 2008; Landschützer et al., 2016). Interannual trends in summer variability of ΔpCO_2 are consistent with chlorophyll-*a* variability where the latter had high mean seasonal concentrations.~~We separate the analysis of the ΔpCO_2 and its drivers into summer and winter. We find that understanding the variability of ΔpCO_2 and its drivers on shorter time scales is critical to resolving the long-term variability of ΔpCO_2. Results show that ΔpCO_2 is rarely driven by thermodynamics during winter, but rather by mixing and stratification due to the stronger correlation of ΔpCO_2 variability with mixed layer depth. Summer pCO_2

variability is consistent with chlorophyll-*a* variability, where higher concentrations of chlorophyll-*a* correspond with lower pCO_2 concentrations. In regions of low chlorophyll-*a* concentrations, wind stress and sea surface temperature emerged as stronger drivers of ΔpCO_2. In summary we propose that sub-decadal variability is explained by summer drivers, while winter variability contributes to the long~~-~~-term changes associated with the SAM. This approach is a useful framework to assess the drivers of ΔpCO_2 but would greatly benefit from improved estimates of ΔpCO_2 and a longer time series.

1 Introduction

The Southern Ocean plays a key role in the uptake of anthropogenic CO_2 (Khatiwala et al., 2013; DeVries et al., 2017). Moreover, it has been shown that the Southern Ocean is sensitive to anthropogenically influenced climate variability, such as the intensification of the westerlies (Le Quéré et al., 2007; Lenton et al., 2009; Swart and Fyfe, 2012; DeVries et al., 2017). Until recently, the research community has not been able to ~~accurately measure~~quantify the contemporary changes~~, let alone understand the drivers,~~ of CO_2 in the Southern Ocean accurately due to a paucity of observations, let alone understand the drivers (Bakker et al., 2016). Empirical models provide an interim solution to this challenge until prognostic ocean biogeochemical models are able to represent ~~the~~ Southern Ocean CO_2 ~~seasonal cycle accurately~~fluxes adequately (Lenton et al., 2013; Rödenbeck et al., 2015; Mongwe et al., 2016). The research community agrees on large changes in CO_2 fluxes in the Southern Ocean from a ~~source in the 1990's to a~~ weakening sink in the ~~2000's~~1990s to a strengthening sink in the 2000s; however, there is disagreement ~~in~~over the drivers of the changes in CO_2 uptake (Lovenduski et al., 2008; Landschützer et al., 2015; DeVries et al., 2017~~).~~; Ritter et al., 2017). This study aims to understand the drivers of the changing CO_2 sink in the Southern Ocean, based on an ensemble of empirical estimates using a seasonal analysis framework.

Empirical methods estimate CO_2 by extrapolating ~~the~~ sparse ship~~-~~-based CO_2 measurements using proxy variables. The proxies are often satellite observable ~~proxies. This approach has allowed for a better~~but may include climatologies or output from assimilative models. Empirical methods have improved our understanding of ~~the drivers of~~ CO_2 trends in the Southern Ocean by ~~providing improved spatial and temporal resolution~~increasing the data coverage. However, there is still disagreement between many of the ~~variability.~~methods due to the paucity of data and the way in which each method interpolates sparse data (Rödenbeck et al., 2015; Ritter et al., 2017).

In a key study, Landschützer et al. (2015) showed, using an artificial neural network (ANN), that there was significant strengthening of Southern Ocean CO_2 uptake during the period ~~2000~~2002-2010. While previous studies suggested that changes in wind strength have led to changes in meridional overturning and thus CO_2 uptake (Lenton and Matear, 2007; Lovenduski et al., 2007; Lenton et al., 2009; DeVries et al., 2017), Landschützer et al. (2015) suggested that atmospheric circulation has become more zonally asymmetric since the mid ~~2000's~~2000s, which has led to an oceanic dipole of cooling and warming. The net impact of cooling and warming, together with changes in the DIC/TA (Dissolved Inorganic Carbon/Total Alkalinity), led to an increase in the uptake of CO_2 (Landschützer et al., 2015). During this period, southward advection in the Atlantic basin~~, southward advection~~ reduced upwelled DIC in surface waters~~,~~ overcoming the effect of the concomitant warming in the region. Conversely, in the Eastern Pacific sector of the Southern Ocean, strong cooling overwhelmed increased upwelling (Landschützer et al., 2015). ~~Munro et al. (2015)~~This is supported ~~this mechanism, with data~~by observations from the Drake Passage and south of Australia showing that ~~Δ~~variability of upwelling has affected Δ pCO_2 ~~decreased between 2002 and 2014.~~(Munro et al., 2015; Xue et al., 2015).

In a subsequent study, Landschützer et al. (2016) proposed that interannual variability of CO_2 in the Southern Ocean is tied to the decadal variability of the Southern Annular Mode (SAM) – the dominant mode of atmospheric variability in the Southern Hemisphere (Marshall, 2003). This concurs with previous studies, which suggested that the increase in the SAM during the ~~1990's~~1990s resulted in the weakening of the Southern Ocean sink (Le Quéré et al., 2007; Lenton and Matear, 2007; Lovenduski et al., 2007; Lenton et al., 2009~~).~~; Xue et al., 2015). The work by Fogt et al. (2012) bridges the gap between the proposed asymmetric atmospheric circulation of Landschützer et al. (2015) and the observed correlation with the SAM of Landschützer et al. (2016). Fogt et al. (2012) show that changes in the SAM have been zonally asymmetric and that this variability is highly seasonal, thus amplifying or suppressing the amplitude of the seasonal mode.

Assessing the changes through a seasonal framework may thus help shed light on the drivers of CO_2 in the Southern Ocean. Southern Ocean seasonal dynamics suggest that the processes driving ~~Δ~~pCO_2 are complex~~,~~ but with two clear contrasting extremes. In winter, the dominant deep mixing and entrainment processes are zonally uniform~~,~~ driving an increase in ~~Δ~~pCO_2, with the region south of the Polar Front (PF) becoming a net source and weakening the net sink north of the PF (Lenton et al., 2013). In summer, the picture is more spatially heterogeneous, with net primary production being the primary driver of variability (Mahadevan et al., 2011; Thomalla et al., 2011; Lenton et al., 2013). The ~~competition~~competing influence between light and iron limitation results in heterogeneous distribution of chlorophyll-*a* (Chl-*a*) in both space and time, with similar implications for ~~Δ~~pCO_2 (Thomalla et al., 2011; Carranza and Gille, 2015). The interaction between the large-scale drivers, such as wind stress, surface heating and mesoscale ocean dynamics, ~~is~~are the primary cause of this complex picture (McGillicuddy, 2016; Mahadevan et al., 2012). Some regions of elevated mesoscale and submesoscale dynamics, mainly in the Sub-Antarctic Zone (SAZ~~)~~), are also characterized by strong intraseasonal modes in summer primary production~~-~~ and pCO_2 (Thomalla et al., 2011; Monteiro et al., 2015). In general, the opposing effects of mixing and primary production result in the seasonal cycle being the dominant mode of variability in the Southern Ocean (Lenton et al., 2013).

In this study we examine winter and summer interannual variability of ΔpCO_2 ~~from 1998 to 2014~~ in the Southern Ocean between 1998 – 2014 to understand the drivers of long~~-~~-term changes in CO_2 uptake.

~~2 Empirical methods and data~~

2 Methodology

2.1 Empirical methods and data

In this study we use three machine~~-~~-learning methods: Random Forest Regression (RFR), Support Vector Regression (SVR) and Self-Organising-~~Maps~~Map Feed-Forward Neural Network (SOM-FFN). RFR and SVR are introduced in Gregor et al. (2017) and SOM-FFN is presented in Landschützer et al. (2014). In brief, the RFR approach is an ensemble of decision trees that provides non-linear regression by combining many high variance – low bias estimators (Gregor et al., 2017). SVRs are in principle similar to a single hidden layer FFN, ~~with the difference~~except that SVR statistically determines the complexity of the problem, which is analogous to the hidden layer structure that is typically determined heuristically. The SOM-FFN method is a two-step neural network approach that first clusters data (SOM) and then applies a regression model (FFN) to each cluster.

The SVR and RFR implementations used in this study are trained with the monthly 1° by 1° gridded SOCAT (Surface Ocean CO_2 Atlas) v3 dataset (Bakker et al., 2016). The SOM-FFN (~~v2.2~~run ID: *netGO5*) used in this study was trained with SOCAT v4 (Landschützer et al., 2017).

Table 1: Three empirical methods used in the ensemble. RFR and SVR are described in Gregor et al. (2017). SOM-FFN is from Landschützer et al. (2016). SST = sea surface temperature, MLD = mixed layer depth, SSS = sea surface salinity, ADT = absolute dynamic topography, Chl-*a* = Chlorophyll-*a*, $pCO_{2(atm)}$ = fugacity of atmospheric CO_2, $xCO_{2(atm)}$ = mole fraction of atmospheric CO_2, ~~Φ(~~Φ (lat, lon) = *N*-vector transformations of latitude and longitude, *t*(day of year) = trigonometric transformation of the day of the year. Note that SOM-FFN uses the de Boyer Montégut et al. (2004) climatology for MLD (dBM2004). The root mean squared errors (RMSE) listed in the last column are for the Southern Ocean from Gregor et al. (2017).

Method	Input variables	RMSE (µatm)
RFR	SST, MLD, SSS, ADT, Chl-$a_{(clim)}$, $pCO_{2(atm)}$, Φ(lat, lon), *t*(day of year)	16.45
SVR	SST, MLD, SSS, ADT, Chl-$a_{(clim)}$, $pCO_{2(atm)}$, Φ(lat, lon), *t*(day of year)	24.04
SOM-FFN	SST, $MLD_{dBM2004}$, SSS, Chl-*a*, $xCO_{2(atm)}$	14.84

Table 1 shows the proxy variables used for each of the methods. Sea surface salinity (SSS) and mixed layer depth (MLD) for SVR and RFR are from Estimating the Circulation and Climate of the Ocean, Phase II ($ECCO_2$) (Menemenlis et al., 2008). The use of these assimilative modelled products may in some cases produce results that are unrealistic. This may have influenced the use of the de Boyer Montégut et al. (2004) MLD climatology in the SOM-FFN, where $ECCO_2$ was used in previous iterations of the product. The trade-off of using the climatology is that no interannual changes in MLD are taken into account. We acknowledge that using different proxy variables could result in different $\Delta p CO_2$ estimates, but comparing the different proxies used in each of the CO_2 products is beyond the scope of this study. Other data sources that are consistent between methods are: sea surface temperature (SST) and sea-ice fraction by Reynolds et al. (2007), ~~Chlorophyll-*a* (~~Chl-*a*~~)~~ by Maritorena and Siegel (2005), absolute dynamic topography (ADT) by ~~-~~Duacs, and xCO_2 (CDIAC, 2016) with $pCO_{2(atm)}$ calculated from interpolated xCO_2 using NCEP2 sea level pressure (Kanamitsu et al., 2002). In the case of Chl-*a* for SVR and RFR, Gregor et al. (2017) filled the cloud gaps with climatological Chl-*a*. Note that ADT coverage is limited to regions of no to very low concentrations of sea-ice cover, ~~thus~~so estimates for SVR and RFR ~~methods~~ do not extend into the ice~~-~~-covered regions during winter. Our analyses are thus limited to the ~~regions without~~ region north of the maximum sea-ice ~~cover~~extent.

Seasonality of the data is preserved by transforming the day of the year (j) and is included in both SVR and RFR analyses:

$$t = \begin{pmatrix} \cos\left(j \cdot \frac{2\pi}{365}\right) \\ \sin\left(j \cdot \frac{2\pi}{365}\right) \end{pmatrix} \tag{1}$$

Transformed coordinate vectors are passed to SVR only using n-vector transformations of latitude (λ) and longitude (μ) (Gade, 2010; Sasse et al., 2013), with n containing:

$$\cancel{N = \begin{pmatrix} \sin(\lambda) \\ \sin(\mu) \cdot \cos(\lambda) \\ -\cos(\mu) \cdot \sin(\lambda) \end{pmatrix} \quad (2)}$$

Wind speed, while not used in the empirical methods, is used in the assessment of the drivers of CO_2. We use CCMP v2, which is an observation-based product that combines remote sensing, ship and weather buoy data (Atlas et al., 2011). Swart et al. (2015a) compared a number of wind reanalysis products with CCMP v1 (where CCMP was the benchmark). The authors found that many of the reanalysis products had spurious trends, particularly in the Southern Hemisphere where data is sparse. Our choice of CCMP, which is based on observations, ~~is thus one that~~ aims to minimise the assumptions that are otherwise made by reanalysis products.

2.2 Uncertainties

The machine-learning approaches used in this study are by no means able to estimate ΔpCO_2 with absolute certainty. To account for the uncertainty, we use the same approach as Landschützer et al. (2014) to calculate total errors for each of the methods:

$$\boldsymbol{e}_{(t)} = \sqrt{e_{meas}^2 + e_{grid}^2 + e_{map}^2} \tag{3}$$

where $e_{m(t)}$ is the total error associated with a method (m); e_{meas} is the error associated with SOCAT measurements, which is fixed at 5 µatm (Pfeil et al., 2013); e_{grid} is the 5 µatm error associated with gridding the data into monthly by 1° bins (Sabine et al., 2013). Lastly e_{map} is the root mean squared error (RMSE) calculated for each method, as shown in Table 1 taken from Gregor et al. (2017).

These errors are used to calculate the average "within-method" error as defined by Gurney et al. (2004):

$$\mathrm{E}_w = \sqrt{\frac{1}{M} \cdot \sum_{m=1}^{M} (e_{m(t)})^2} \tag{4}$$

where $e_{m(t)}$ is the method-specific error as defined in Equation ~~1~~3 and M is the number of methods (3 in this case). For a measure of the difference between methods we use the "between-method" approach used in Gurney et al. (2004):

$$E_b = \sqrt{\frac{1}{M} \sum_{m=1}^{M} (S_m - \bar{S})^2} \tag{5}$$

where S_m is the method estimate of ΔpCO_2 and $\bar{S}$ is the mean of the methods. This is analogous to the standard deviation (for a known population size). We later use an adaptation of this metric as a threshold to determine the confidence around anomalies.

2.3 Regional Coherence Framework

Southern Ocean CO_2 is spatially heterogeneous, both zonally and meridionally (Jones et al~~.~~., 2012). In order to understand this heterogeneity, we used the three southernmost biomes defined by Fay and McKinley (2014a~~)~~), as done in Rödenbeck et al. (2015). From north to south these are~~:~~ the subtropical seasonally stratified (STSS), sub-polar seasonally stratified (SPSS~~),~~) and seasonally ice-covered region (ICE). These three biomes are comparable to the SAZ (Sub-Antarctic Zone), PFZ (Polar-Frontal Zone) and MIZ (Marginal Ice Zone) respectively and will be used throughout the rest of the study. The Southern Ocean is further split into basins where the boundaries are defined by lines of longitude (70°W : Atlantic : 20°E : Indian : 145°E : Pacific : 70°W). ~~Figure 1 depicts these nine regions.~~

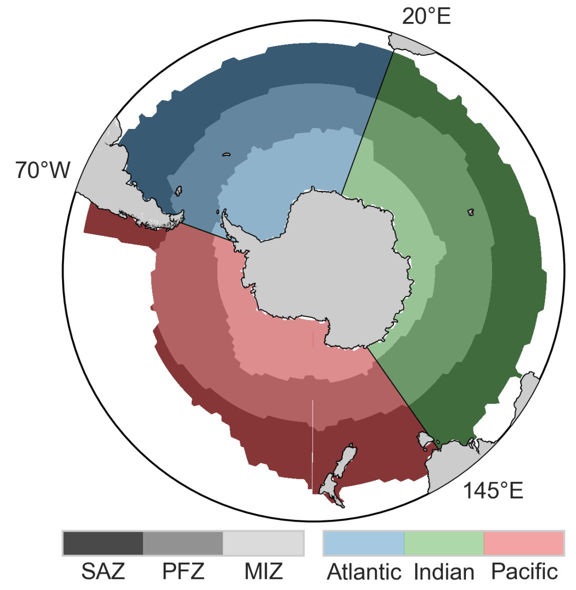

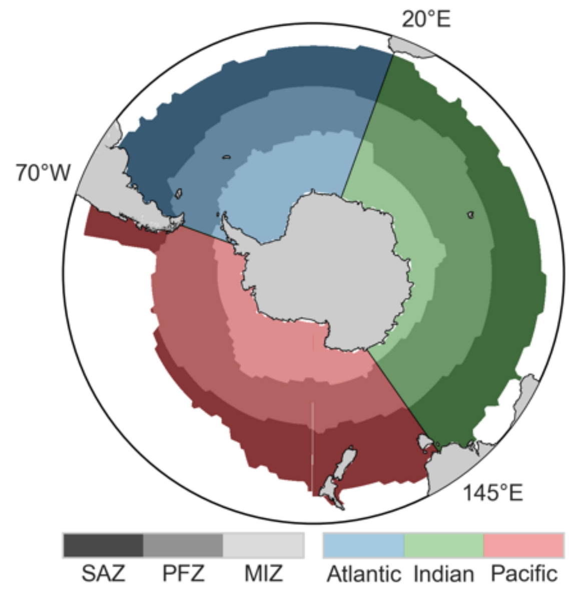

Figure 1: A map showing the regions used throughout this study. The three biomes, SAZ, PFZ and MIZ, used in this study are defined by Fay and McKinley (2014a). The regions are also split by basin.

3 Results and discussion

~~Here we present and discuss the results.~~ The first section of the results examines the uncertainties of the ensemble and its members. We then ~~consider~~look at the seasonal cycle of the ensemble mean in time and space. This is done to lay the foundation for the interpretation of the results when assessed with the regional framework. In the regional interpretation the ~~data is~~estimates are decomposed into ~~the~~ nine regions, as shown in Figure 1. Lastly, we implement a seasonal decomposition of the estimates to interpret the drivers of the changes observed in $\Delta p\mathrm{CO_2}$.

3.1 Ensemble member performance and variability

Table 2: A regional summary of the errors for the different ~~models~~methods. Note that the propagated errors are calculated as shown in equation (3) where the measurement and gridding errors are assumed to be constant at 5 µatm each (Pfeil et al., 2013; Sabine et al., 2013). The within-~~model~~method and between ~~model~~method errors are calculated using equations (4) and (5) respectively.

Biome	Propagated errors (µatm)			Within ~~model~~method error (µatm)	Between ~~model~~method error (µatm)
	SVR	RFR	SOM-FFN		
SAZ	17.48	14.50	12.30	14.91	4.88
PFZ	15.94	12.71	13.09	13.99	4.78
MIZ	36.38	24.53	22.46	28.46	10.81
Southern Ocean	**25.06**	**17.91**	**16.44**	**20.16**	**6.79**

We use the RMSE scores as presented in Gregor et al. (2017) with abbreviated results shown in Table 1. The SOM-FFN method has the best score (14.84 µatm). SVR scores the lowest (24.04 µatm), but ~~was~~is still included due to the method's sensitivity to sparse data, which is favourable to the poorly sampled winter period (Gregor et al~~.~~., 2017). This compliments the RFR method, which scores well (16.45 µatm~~),~~) but is prone to being insensitive to sparse data (Gregor et al~~.~~., 2017). These RMSE scores are used to calculate the total errors for each method and region using equation (3~~)~~), where the measurement and mapping errors are both 5 µatm each (Pfeil et al., 2013; Sabine et al., 2013). These results are shown in Table 2.

Total errors are used to calculate the within-method error, which is an estimate of the combined total ~~errors~~error of the three machine~~-~~-learning methods (equation 4). The between-method errors are the mean of the standard deviation between the methods (equation 5). The within-method errors are much larger than the between-method errors (Table 2). However, the within-method errors are normally distributed and are mechanistically consistent (Gregor et al., 2017). ~~This allows us to observe changes that are smaller than the within-method error.~~ The between-method error (shown in Figure ~~2d) serves as a better measure of~~2c) is thus used to determine whether observed variability is ~~more than statistical noise as it incorporates~~consistent between the three ~~methodologically different approaches.~~ methods.

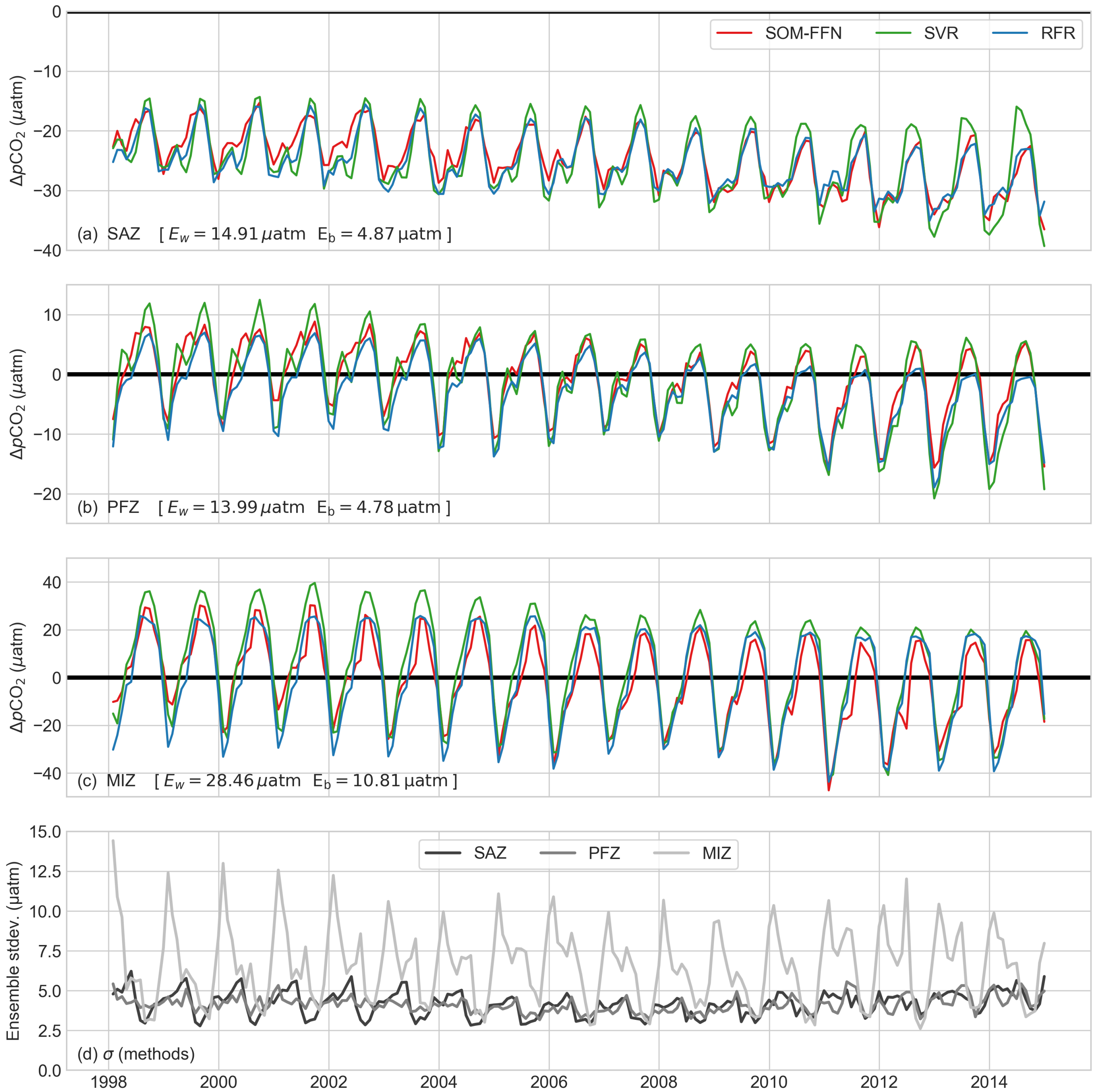
SOM-FFN
SVR
RFR
ΔpCO2 (μatm)
(a) SAZ [$E_w = 14.91\,\mu$atm $E_b = 4.87\,\mu$atm]
(b) PFZ [$E_w = 13.99\,\mu$atm $E_b = 4.78\,\mu$atm]
(c) MIZ [$E_w = 28.46\,\mu$atm $E_b = 10.81\,\mu$atm]
SAZ
PFZ
MIZ
Ensemble stdev. (μatm)
(d) σ (methods)
1998
2000
2002
2004
2006
2008
2010
2012
2014

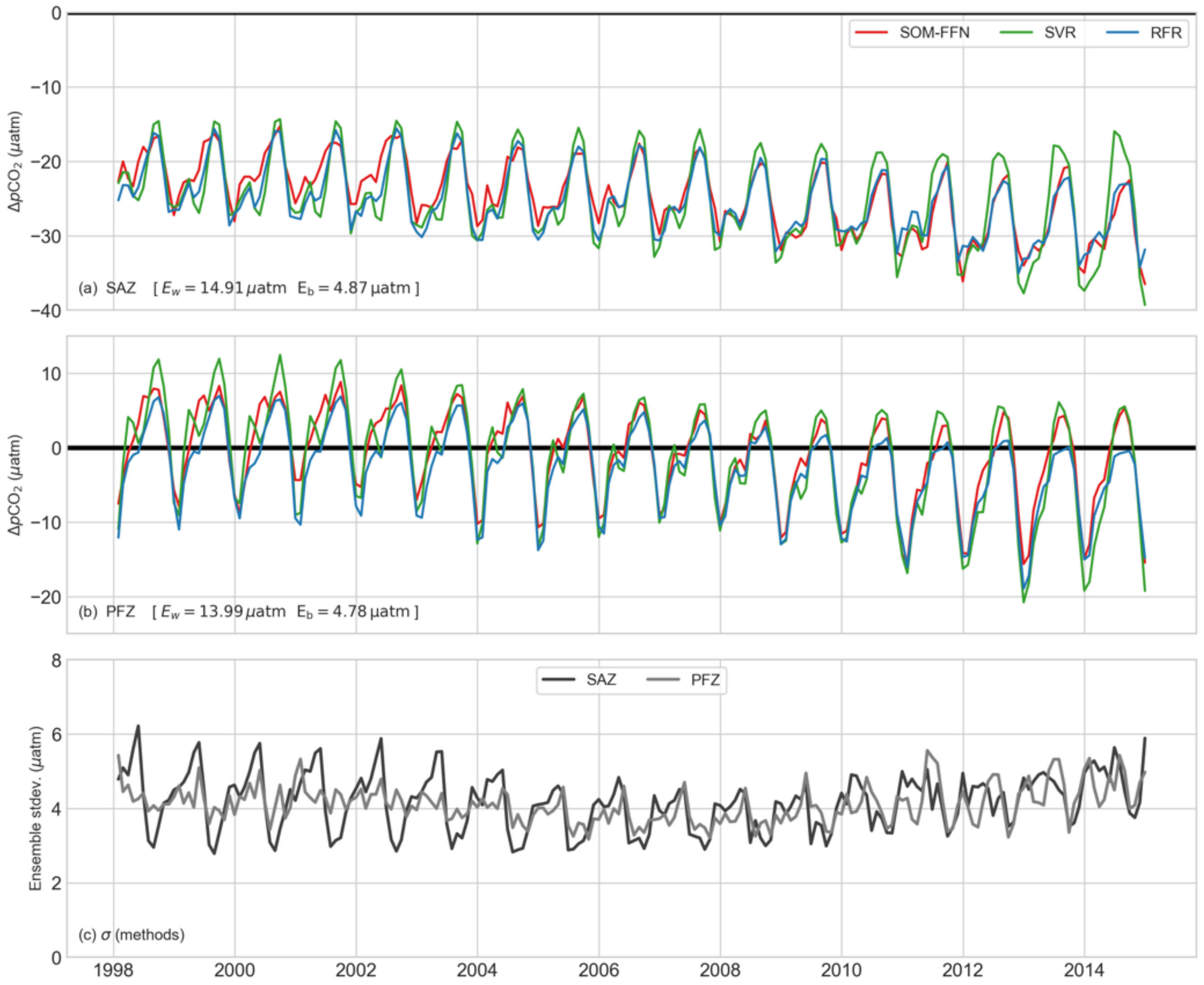

Figure 2: Time series of the three ensemble ~~members~~methods for each biome, as defined by Fay and McKinley (2014a): (a) SAZ, (b) PFZ, (c) ~~MIZ. (d) shows~~ the standard deviation between ensemble members for the three biomes, which is analogous to the between-~~model~~method error (equation 5). The within-method (E_w) and between-method (E_b) errors are shown for each biome. For a more detailed breakdown of the errors see Table 2.

Figure 2 shows the ΔpCO_2 time series for ~~each of the methods for~~the SAZ and PFZ. Note that we exclude the ~~three Southern Ocean biomes. The methodological and data driven differences~~ MIZ from the remaining analyses due to large E_b and E_w (Table 2) and inconsistent coverage between ~~each of the methods have been addressed~~products due to sea-ice cover (MIZ data is shown in ~~Gregor et al. (2017).~~the supplementary materials S2, S3). In general, there is good agreement amongst the methods ~~with a few notable exceptions.~~and the magnitude of these differences is within the average within-method error (E_w), but the differences are important to highlight as they contribute to the between-method error (E_b). In the SAZ (Figure 2a~~)~~), the SOM-FFN differs from the other methods for summer and autumn from 1998 to 2008. ~~Gregor et al. (2017) attributed this difference to the clustering step in the SOM-FFN that creates discrepancies in the Atlantic sector.~~ The SVR method overestimates the seasonal amplitude ΔpCO_2 (where the seasonal amplitude is the difference between the winter maxima and summer minima of ΔpCO_2) relative to the other methods for 2012 to 2014. In the PFZ (Figure 2b), the SVR overestimates ΔpCO_2 relative to the other methods during winter from 1998 to 2004, likely due to the method's sensitivity to sparse winter data (Gregor et al., 2017). ~~. These differences contribute to the between-method error.~~

~~The seasonal amplitude of $\Delta p CO_2$ in the MIZ is much larger than the two other regions. However, this amplitude is likely to be dampened by ice cover (Ishii et al., 1998; Bakker et al., 2008; Butterworth and Miller, 2016). Note that in this study, we do not include regions with sea-ice cover to ensure consistency between methods. Calculated fluxes for this methodologically reduced region will thus under-represent the fluxes of the full extent of the MIZ. We thus exclude the MIZ for the remainder of the study.~~

Figure ~~2d~~2(c) shows the time evolution of between-method errors for each biome. This panel highlights the seasonality of the ~~data~~estimates, specifically the increased heterogeneity of $\Delta p CO_2$ in summer and the impact ~~that~~ this has on $\Delta p CO_2$ estimates. This is due to the more complex competing processes affecting ~~Δ~~pCO_2 during summer. To gain a better understanding of the seasonal processes, we ~~look at~~consider the mean state of each season to characterise the drivers of opposing fluxes.

3.2 Ensemble seasonal cycle

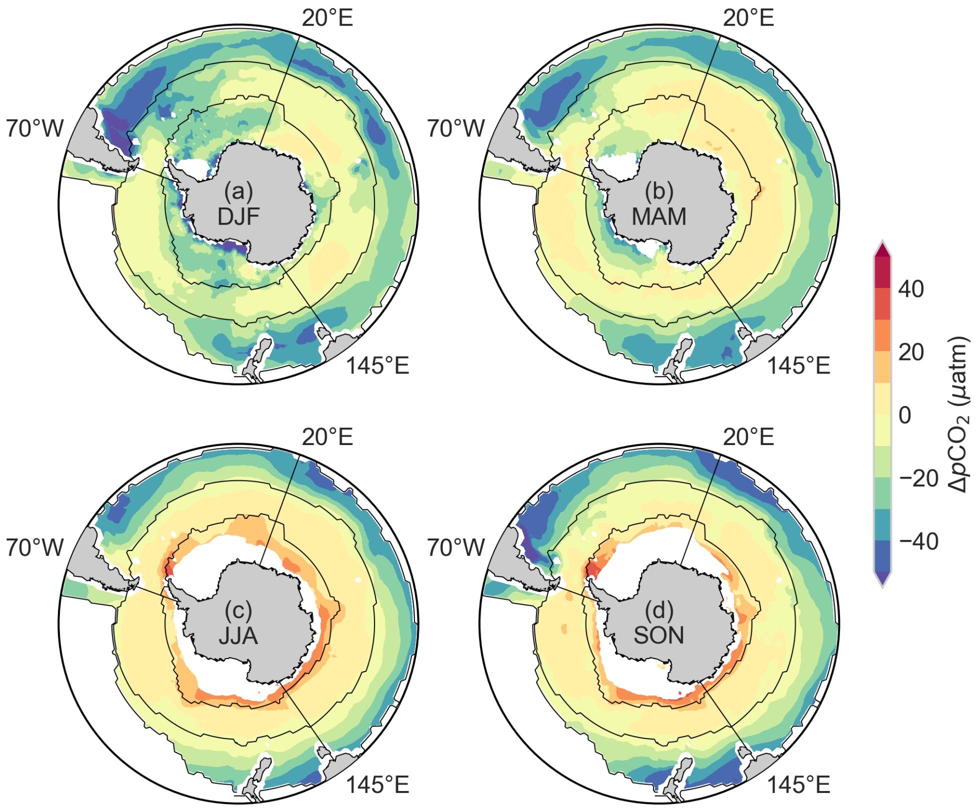

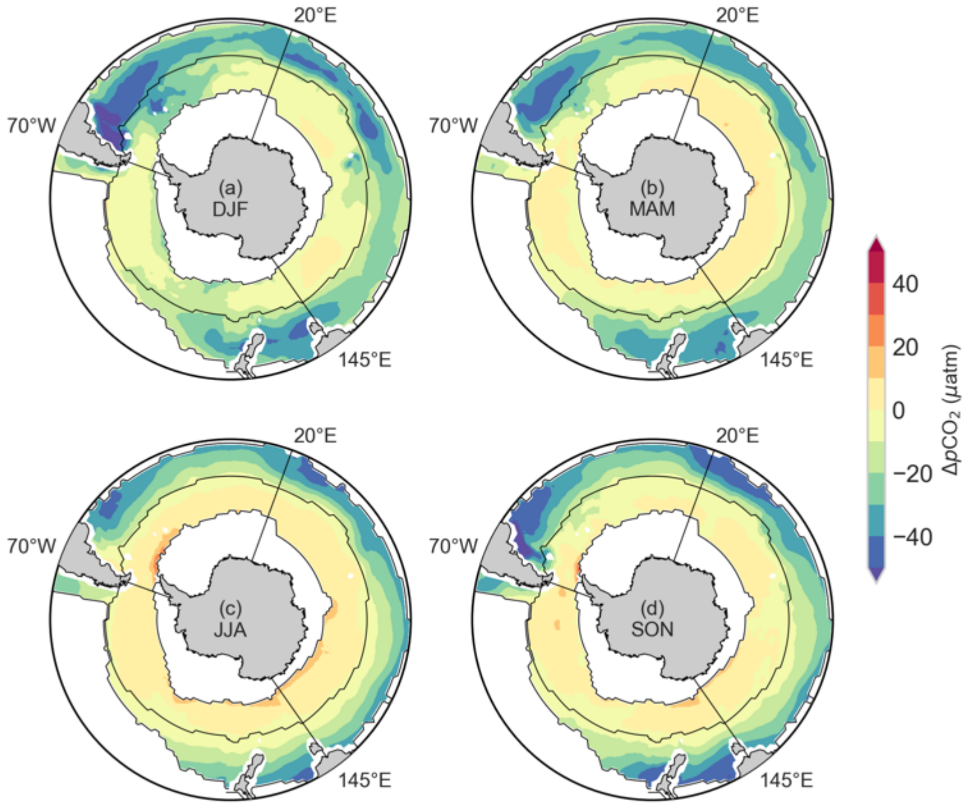

Figure 3: The mean seasonal states of ΔpCO$_2$ of the empirical ensemble mean. These are shown for (a) summer, (b) autumn, (c) winter and (d) spring. The black contour lines show the SAZ, PFZ and MIZ (masked) from north to south, as defined by Fay and McKinley (2014a).

The seasonal cycle of the ΔpCO$_2$ for each biome (Figure 2a-~~e~~b and Figure 3a-~~e~~d) is coherent with seasonal processes reported in the literature (Metzl et al., 2006; Thomalla et al., 2011; Lenton et al., 2012; Lenton et al., 2013). In all biomes, uptake of CO_2 is stronger during summer than in winter, giving rise to the strong seasonal cycle. This is due to the opposing influences of the dominant winter and summer drivers, partially damped by the seasonal cycle of temperature (Takahashi et al., 2002; Thomalla et al., 2011; Lenton et al., 2013). ~~The~~In winter, the dominant processes of mixing and entrainment ~~in winter result~~results in increased surface $p\mathrm{CO}_2$ and thus outgassing (Takahashi et al., 2009; Lenton et al., 2013; Rodgers et al., 2014). In summer, stratification~~ also~~ allows for increased biological production and the consequent uptake of CO_2, thus reducing the entrained winter DIC and associated $p\mathrm{CO}_2$ (Bakker et al., 2008; Thomalla et al., 2011). However, stratification typically limits entrainment~~, but does not exclude the occurrence of entrainment~~ other than during periods of intense mixing driven by storms. This has an impact on primary productivity, DIC and $p\mathrm{CO}_2$ (Lévy et al., 2012; Monteiro et al., 2015; Nicholson et al., 2016; Whitt et al., 2017).

The SAZ (Figure 2a) is a continuous sink, where summer uptake (Figure 3a) is enhanced by biological production and winter (Figure 3c) mixing results in a weaker sink (Metzl et al., 2006; Lenton et al., 2012; Lenton et al., 2013). The same processes produce a similar seasonal amplitude in the PFZ (Figure 2b), but stronger upwelling and weaker biological uptake result in a positive shift of the mean. This results in an opposing net summer sink and winter source. However, this is according to the mean state in the PFZ and winter estimates of $\Delta p\mathrm{CO}_2$ do in fact approach 0 µatm toward the end of the time series (Figure 2b). ~~The MIZ has the strongest seasonal cycle due to upwelling of CO_2 during winter and strong biological uptake in summer. However, much of this is dampened by sea ice cover during winter and weaker winds during summer (Ishii et al., 1998; Bakker et al., 2008).~~

Apparent also from Figure 3 is that, over and above the latitudinal gradient, $\Delta p\mathrm{CO}_2$ is zonally asymmetric within each biome during summer (Figure 3a), when biological uptake of CO_2 increases. Zonal integration of $\Delta p\mathrm{CO}_2$ could thus dampen magnitudes of regional $\Delta p\mathrm{CO}_2$. A regional approach is therefore needed to examine the regional characteristics of seasonal and interannual variability of $\Delta p\mathrm{CO}_2$ and to understand its drivers.

3.3 Regional $\Delta p\mathrm{CO}_2$ variability: zonal and basin contrasts

~~Here~~In Figure 4, $\Delta p\mathrm{CO}_2$ is decomposed into nine domains by biome and basin, with the boundaries ~~shown~~defined in Figure 1~~, but note only six are shown~~ (showing the SAZ and PFZ; air-sea CO_2 fluxes displayed in Figure ~~4.~~S3). The ~~data~~regional estimates are plotted as time series for ~~$p\mathrm{CO}_2$ (Figure 4) showing: mean annual~~ $\Delta p\mathrm{CO}_2$ (black lines~~), the maximum~~). The blue and orange lines show the respective annual maxima (typically winter~~ values (red line~~) and ~~the projected summer~~ minima (~~dashed red line~~typically summer). The projected summer minima (dashed blue lines) are calculated by subtracting the mean seasonal amplitude from the winter maxima (Figure 4~~, with air-sea CO_2 fluxes shown in Figure~~

~~S3).~~). The projected summer minima are the expected summer $\Delta p CO_2$ under the assumption that summer $\Delta p CO_2$ is dependent on, but not restricted to, the baseline set by winter. ~~Differences between the summer minima and projected minima are highlighted with green and blue patches, highlighting periods of decoupling between summer and winter interannual variability. The green areas indicate periods of strong uptake (relative to winter) that enhance the mean uptake of CO_2 and amplify the seasonal cycle. Conversely, blue areas show periods where weak summer uptake (relative to winter) offsets winter outgassing, thus reducing the mean $\Delta p CO_2$ as well as supressing the amplitude of the seasonal cycle (Figure 4).~~

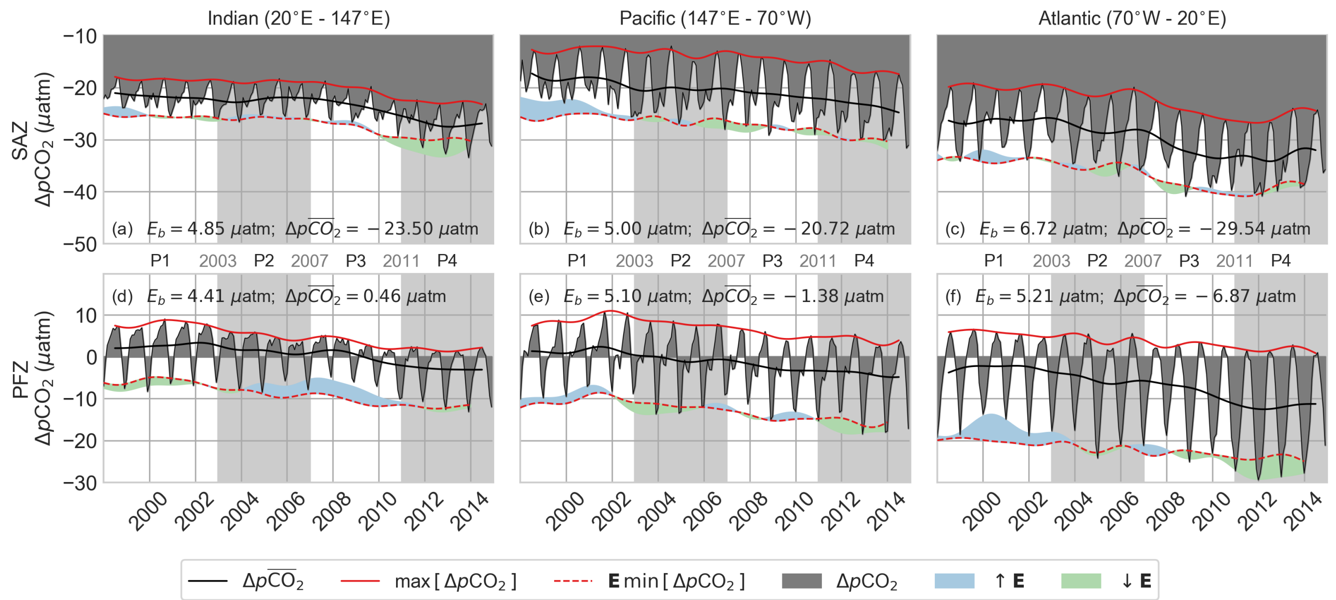

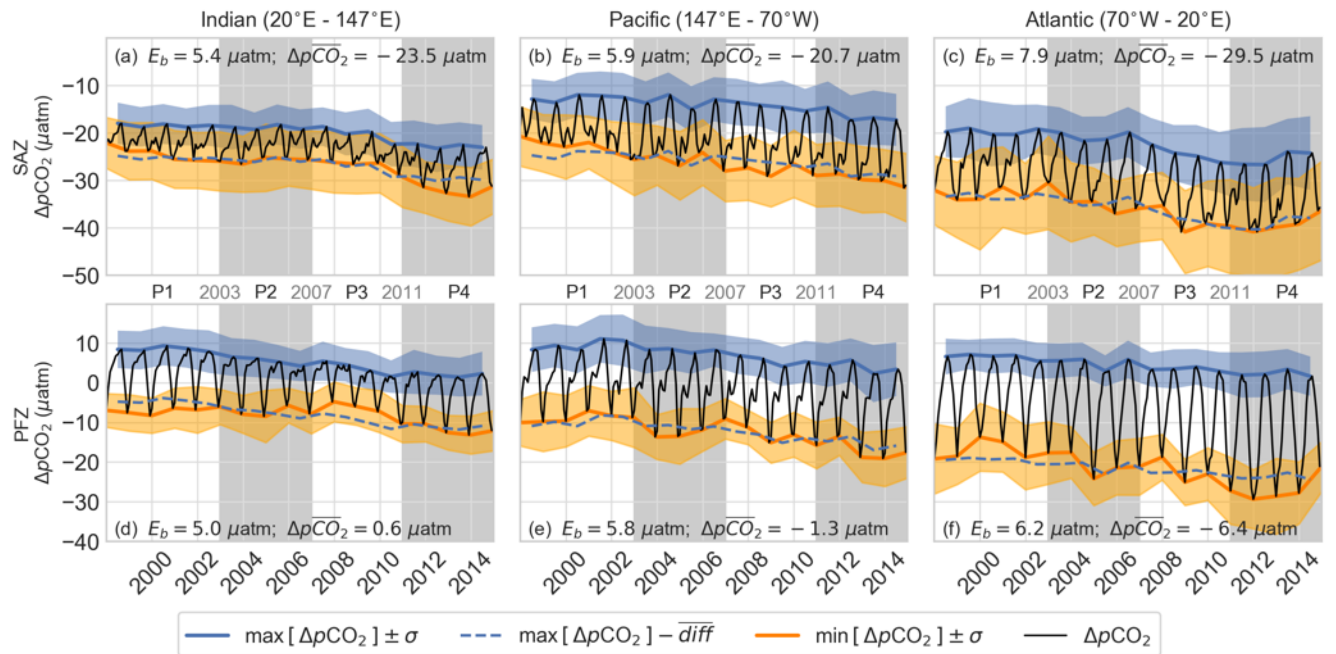

Figure 4: Figures (a-f) show the ensemble mean of $\Delta p CO_2$ (~~dark grey~~black) plotted by biome (rows) and basin (columns). Biomes are defined by Fay and McKinley (2014a). The ~~solid red~~blue line shows the maximum for each year (winter outgassing) and the dashed blue line shows the same line less the average seasonal amplitude ($diff$) – this is the expected amplitude. ~~The shaded blue (green) area shows when the annual minimum is less (greater) than the expected amplitude~~The orange line shows the minimum $\Delta p CO_2$ for each summer season. The shaded regions around the seasonal maxima and minima show the standard deviation of the three products. E_b is the average between-method error and $\Delta p \overline{CO_2}$ is the average for the entire time series. Light grey shading in (a-f) shows the periods used in Figure 5 and Figure 6.

As found by Landschützer et al. (2015), the estimates of ~~The data for~~ $\Delta p\mathrm{CO_2}$ (Figure 4) show that the Southern Ocean sink ~~strengthened~~strengthens from 2002 to 2011 in all domains, ~~a period identified~~referred to as the *reinvigoration* ~~by Landschützer et al. (2015).~~. This ~~was~~is preceded by a period of a net weakening sink (Figures 4b,d,e) in the ~~1990's~~1990s, referred to as the *saturation* period ~~after~~by Le Quéré et al. (2007). In ~~the period from 2012 to 2014, three domains (Figure 4a,c,f) go from growing uptake to reducing uptake; however, our confidence in~~ other words, the ~~changing~~ensemble shows the same trend ~~is low due to lack of coherence~~found in past literature (Rödenbeck et al., 2015; Ritter et al., 2017), but as with these studies we also find that there is large uncertainty in the interannual variability of the ensemble estimate, as shown by the between-method error in Figure 4 (see Figure S3 for the spread of the product estimates, including the Jena – Mixed Layer Scheme by Rödenbeck et al., 2014). This disagreement between methods ~~(Figure 2a,b)~~is likely driven by the sparse coverage of $p\mathrm{CO_2}$ measurements in the Southern Ocean, with empirical methods interpolating the sparse data differently (Rödenbeck et al., 2015; Ritter et al., 2017). We thus present our methods and ~~only three years of data, with little data in 2014~~results as a framework to assess the drivers of interannual variability of $\Delta p\mathrm{CO_2}$.

~~A key feature of Figure 4 is that~~ Key to understanding the mean interannual variability is that it is the net effect of the decoupled seasonal modes of variability for summer and winter. This is particularly evident in the PFZ (Figures 4d-f). Here, and in the other biomes, the net strengthening of the $\mathrm{CO_2}$ sink is mainly linked to a reduction of $\Delta p\mathrm{CO_2}$ in winter for the majority of the time series. This corresponds with the findings of Landschützer et al. (2016), who linked the reinvigoration to the decadal variability of the Southern Annular Mode (SAM) – the dominant mode of atmospheric variability in the Southern Hemisphere (Marshall, 2003). In contrast, summer $\Delta p\mathrm{CO_2}$ variability is shorter (roughly 4 – 6 years), thus providing ~~inter-annual~~interannual modulation of longer time-scale winter variability. This is demonstrated well in the Indian sector of the PFZ, where a decrease in winter $\Delta p\mathrm{CO_2}$ from 2002 to 2011 is offset by weakening of the summer sink from 2006 to 2010 (Figure 4d). Similarly, in the Atlantic and Pacific sectors of the PFZ, decoupling occurs from ~2011 to the end of 2014, with a rapid increase in the strength of the summer sink.

The mean amplitude of the seasonal cycle of $\Delta p\mathrm{CO_2}$~~,~~ – the mean difference between the summer minima and the winter maxima~~,~~ – is perhaps a better ~~means~~way of understanding the strength of the seasonal drivers than the mean $\Delta p\mathrm{CO_2}$. For example, the Atlantic sectors of the SAZ and PFZ (Figures 4c,f) have the strongest seasonal variability (14.11 and 25.83 µatm respectively). This contrasts with the relatively weak seasonal amplitude in the Indian sector of the Southern Ocean, which has mean amplitudes of 7.06 and 13.64 µatm for the SAZ and PFZ respectively (Figures 4b,e). This contrast can also be seen by comparing the mean seasonal maps of $\Delta p\mathrm{CO_2}$ in Figures 3a and 3c. In summer, strong uptake in the eastern Atlantic sector of the Southern Ocean is indicative of large biological drawdown of CO_2 by phytoplankton (Thomalla et al., 2011). Conversely, relatively low primary production in the Indian sectors of the SAZ and PFZ ~~results~~result in a small seasonal amplitude (Thomalla et al., 2011). This large discrepancy in biological primary production is related to the availability of iron, a micronutrient required for photosynthesis. The lack of large land masses, which are a source of iron, in the Indian sector of the Southern Ocean could be a contributing factor to the lack of biomass (Boyd and Ellwood, 2010; Thomalla et al., 2011).

3.4 Framework: Seasonal deconstruction of interannual variability

Figure 4 gives us insight into the magnitude of interannual $\Delta p\mathrm{CO_2}$ variability as well as the character of these changes; i.e. decoupling of interannual winter and summer modes of variability. This alludes to the point that $\Delta p\mathrm{CO_2}$ is responding to different adjustments of seasonal large~~–~~-scale atmospheric forcing and/or responses of internal ocean dynamics in the Southern Ocean (Landschützer et al., 2015, 2016; DeVries et al., 2017).

In order to capture the decoupled 4–6 year short~~–~~-term variability observed ~~during~~in summer, the ~~data~~estimates are divided into four ~~interannual~~objectively selected periods (P1 to P4~~), where P1 is five years and the remaining~~). The periods ~~(P2 to P4)~~ are each four years ~~as shown by the light grey fills in Figure 4. The small discrepancy in the length~~long with the exception of ~~the periods~~P1, which is five years long due to the ~~uneven length~~fact that the duration of the time series ~~(~~is not divisible by four (with a total duration of 17 years). Given a longer time series, this analysis would benefit from testing different durations for each period, as well as varying the starting and end years.

These four periods are too short for trend analyses (Fay and McKinley, 2014b), but the intention here is to identify periods that are short enough to resolve interannual changes of large-scale drivers of the winter and summer $p\mathrm{CO_2}$ that would otherwise be averaged out over longer periods. We then calculate the relative anomaly between each successive period rather than an anomaly of the mean state (e.g. P2 – P1). As a result, four periods give rise to three sub-decadal-scale transition anomalies for summer and winter: *A* (P2 – P1), *B* (P3 – P2) and *C* (P4 – P3). We do this separately for each method rather than using the ensemble mean (see S4 for calculations). The mean of the method anomalies for each transition is then taken. These anomalies are considered significant if the absolute estimate of the anomaly is larger than the standard deviation between the methods for each period. These calculations along with plots for the standard deviation between methods are shown in ~~the supplementary materials in S4~~section 3.4.1.

Note that~~,~~ although only summer and winter anomalies are discussed, it is recognised that autumn and spring could be equally mechanistically important. Winter anomalies of ΔpCO_2, wind stress, SST and MLD are shown in Figure ~~5. Summer~~ 6, while summer anomalies of ΔpCO_2, wind stress, SST and Chl-*a* are shown in Figure ~~6 where MLD, in winter, is replaced with~~7. Chl-*a* ~~for summer as it~~ is potentially a more important driver in summer than the generally shallow summer MLD (the omitted plots are shown in Figures ~~S5~~S4 and ~~S6~~S5).

3.4.1 Uncertainty of transition anomalies

The transition anomalies are not calculated from the mean of the three products. Rather, we calculate the anomalies for each individual product with:

$$a_{n(p')} = \bar{s}_{n(p)} - \bar{s}_{n(p-1)} \tag{6}$$

where *s* are the estimates for a particular product, *n* represents an individual product and *p* represents P1 to P4. The result, $a_{n(p')}$ thus represents the anomaly for two periods for a particular product. We then calculate the average of the anomalies with:

$$a_{p'} = \frac{1}{N} \cdot \sum_{n=1}^{N} a_{n(p')} \tag{7}$$

where *N* is 3, the number of products. We then calculate the standard deviation of the three anomalies ($e_{p'}$), which is analogous to the between-method error, with:

$$e_{p'} = \sqrt{\frac{1}{N} \cdot \sum_{n=1}^{N} \left(a_{n(p')} - \overline{a_{n(p')}}\right)^2} \tag{8}$$

where the terms are consistent with those above. We use $e_{p'}$ as an uncertainty threshold where anomalies are only considered significant if $|a_{p'}| > e_{p'}$. These regions are masked in Figures 6a-c and 7a-c. Figure 5 shows the winter (a-c) and summer (d-f) $e_{p'}$ for each transition anomaly.

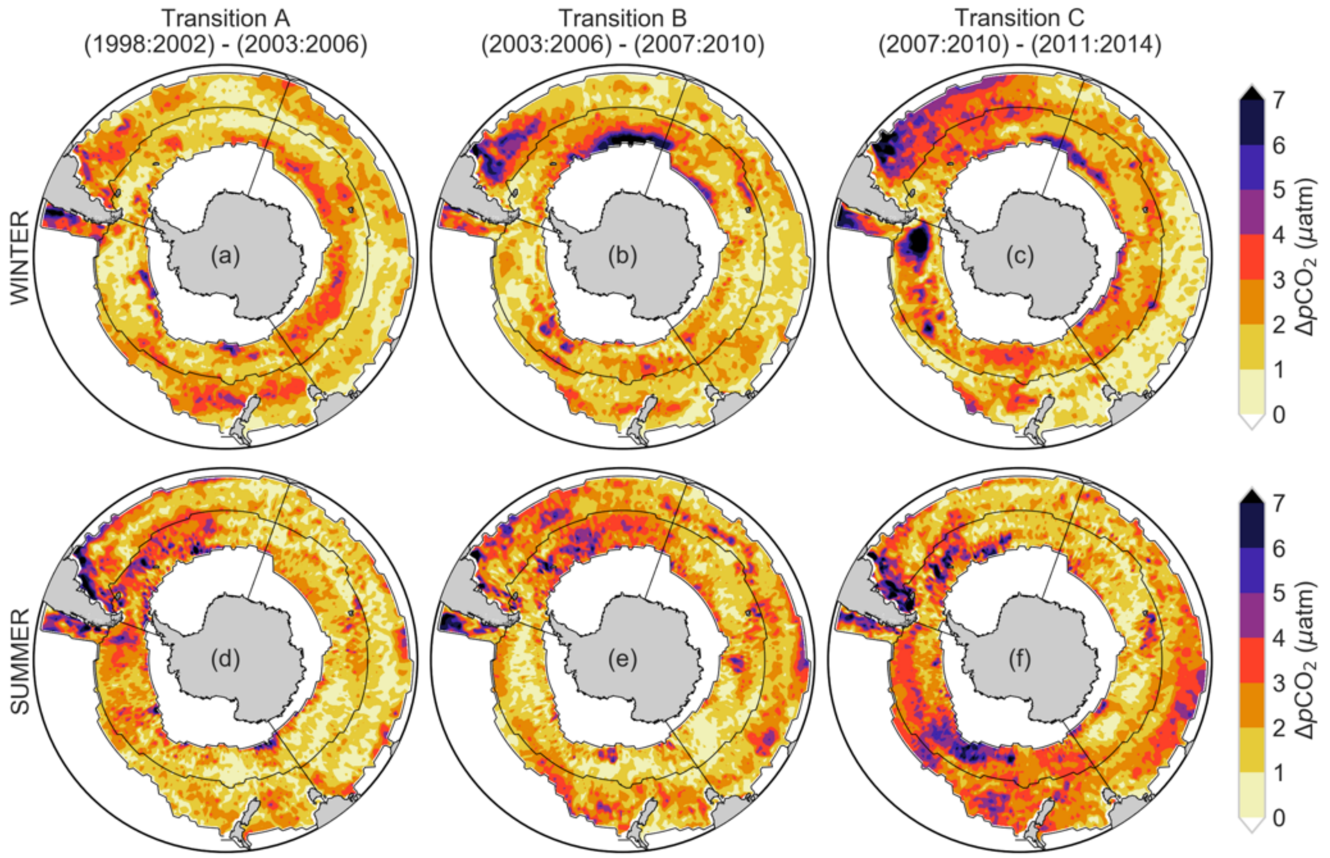

Figure 5: Maps of the standard deviation between empirical methods for the anomalies. These are used as thresholds for $\Delta p CO_2$ in Figures 6(a-c) and 7(a-c) for winter and summer respectively. When the standard deviation exceeds the absolute value average anomaly, the values are masked, as shown in Figures 6 and 7.

3.5 Drivers of winter ΔpCO_2 variability

Figure 6 shows the three transition anomalies for the four periods shown in Figure 4. It is clear that there is large uncertainty around the ΔpCO_2 anomalies in the Southern Ocean owing to the differences between the three empirical methods, caused by a paucity of in-situ measurements of ΔpCO_2. However, there are still small regions that show anomalies with confidence. Figures 6d-l also show the Pearson's correlation coefficients for each of the driver variables with ΔpCO_2 for the regions that are above the uncertainty threshold.

The ~~We will limit the interpretation of the changes to the regions where the anomaly is larger than the between-method error of anomalies (see S4 for calculations and maps). This masks out large regions, but three key points still arise from the significant anomalies. Firstly, ΔpCO_2 is often spatially roughly coherent with wind stress and the inverse of SST. Secondly, there is a dipole in the wind anomalies in the Indian and Pacific between transitions A and B. This is confirmed by the *u*- and *v*-components of wind shown in the supplementary materials (Figure S5). Lastly, the Indian sector of the Southern Ocean dominates the reinvigoration of the CO_2 sink. These points are now addressed in more detail.~~

~~Transition A (P2 – P1) shows a relative increase of ΔpCO_2 in the east Indian and Pacific sectors of the SAZ – suggesting a delay in the onset of the reinvigoration for these basins. This regional sustained saturation corresponds to a shift towards stronger winds and/or deeper MLDs in the west Pacific sector of the SAZ (Figure 5d,j). In contrast, CO_2 uptake in the east Atlantic and west Indian sectors of the SAZ start to strengthen, which roughly corresponds with the weaker winds.~~

~~Transition B (P3 – P2) is characterized by a further intensification of the invigoration of ΔpCO_2 (negative shift) primarily in the Indian basin (Figure 5b). Once again the strengthening of the CO_2 uptake corresponds with weaker wind stress, a warming trend in surface waters and shoaling MLDs in the eastern Atlantic and Indian Ocean sectors of the SAZ and PFZ (Figure 5b,e,h,k). The opposing effects of the dipole are observed east of New Zealand where stronger wind stress, deeper MLD, and cooler surface waters correspond with a positive shift in ΔpCO_2.~~

~~In transition C (P4 – P3), the ΔpCO_2 sink strengthens further in the northern extremes of the east Indian and west Pacific basins. This negative shift corresponds well with strong shoaling of the MLD (Figure~~

~~5l). The west Pacific sector of the PFZ shows a positive shift in ΔpCO_2, which is coherent with an increase in the wind stress and deepening MLD.~~

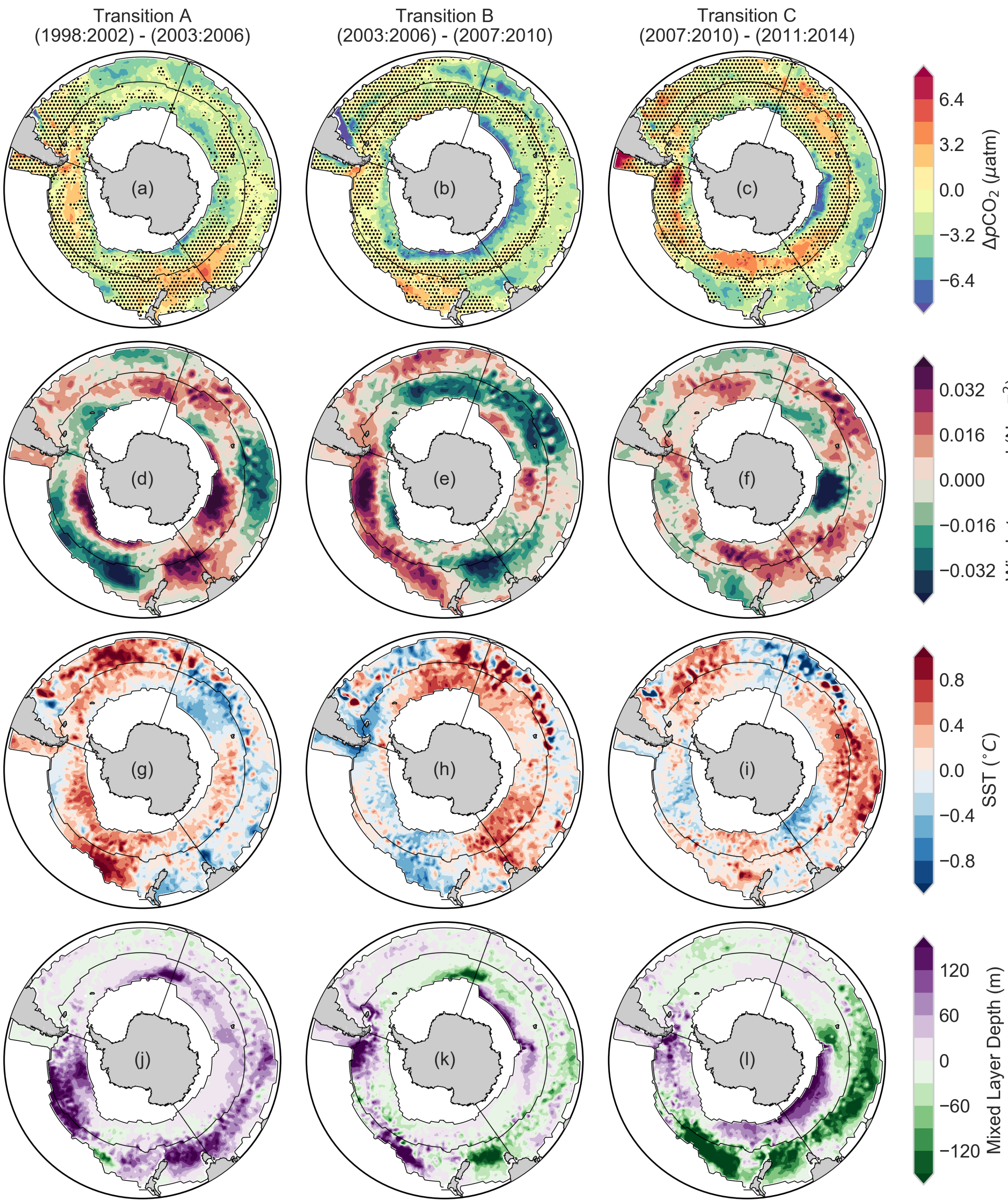

~~Figure 5:~~correlations in Figure 6 show that MLD is a dominant predictor of pCO_2 in winter (Figure 6j-l), with wind stress being a stronger predictor only in Transition B (6e). However, these correlations are all less than |0.3|, indicating that the relationship between ΔpCO_2 and MLD is complex and non-linear. Moreover, spatial inconsistency in the relationship between pCO_2 and the drivers reduce the correlations, which are applied for the entire domain (above the threshold). This is likely due to MLD being a metric that measures the complex interaction of heat, stratification and mixing processes (Abernathy et al., 2011) – mechanisms relating to SST and wind stress. We now discuss the results by transition.

In Transition A (first column of Figure 6), MLD is the strongest driver. Deeper mixed layers in the Pacific and eastern Indian sectors of the Southern Ocean correspond with increased deepening, correlating with increased ΔpCO_2. The reduction of ΔpCO_2 along the boundary of the Atlantic and Indian sectors of the SAZ corresponds with increased SST. This agrees with the hypothesis put forward by Landschützer et al. (2015) that warmer SST in the Atlantic led to increased uptake of CO_2. However, the same is not true for the western Indian sector of the PFZ, where cooling and deepening MLD results in a reduction of ΔpCO_2.

Increased uptake of ΔpCO_2 across the boundary of the Atlantic and Indian sectors of the SAZ continues into Transition B (second column of Figure 6). This is again accompanied by an increase in SST (Figure 6h). The reduction of ΔpCO_2 extends to the Eastern Indian sector of the SAZ and Tasman Sea. This corresponds with weak shoaling of the MLD, weak warming and a reduction of wind stress (Figures 6e,h,k). Conversely, in the eastern Pacific, cooling surface temperatures, weaker winds and shallower MLDs correspond with a reduction of ΔpCO_2, again in agreement with Landschützer et al. (2015). The large reduction of ΔpCO_2 in the Indian sector of the PFZ corresponds with an increase in temperature; however, there is also an increase in the depth of the MLD – this interaction is mechanistically unlikely and may be an artefact of the sparse data in this region.

In transition C, the reduction of ΔpCO_2 in the Indian and western Pacific sector of the SAZ corresponds with warmer SST and shallower MLDs. Once again there is a region in the Indian sector of the PFZ that experiences a potentially spurious reduction of ΔpCO_2 corresponding with deeper MLDs. The anomalies in the rest of the domain are not significant.

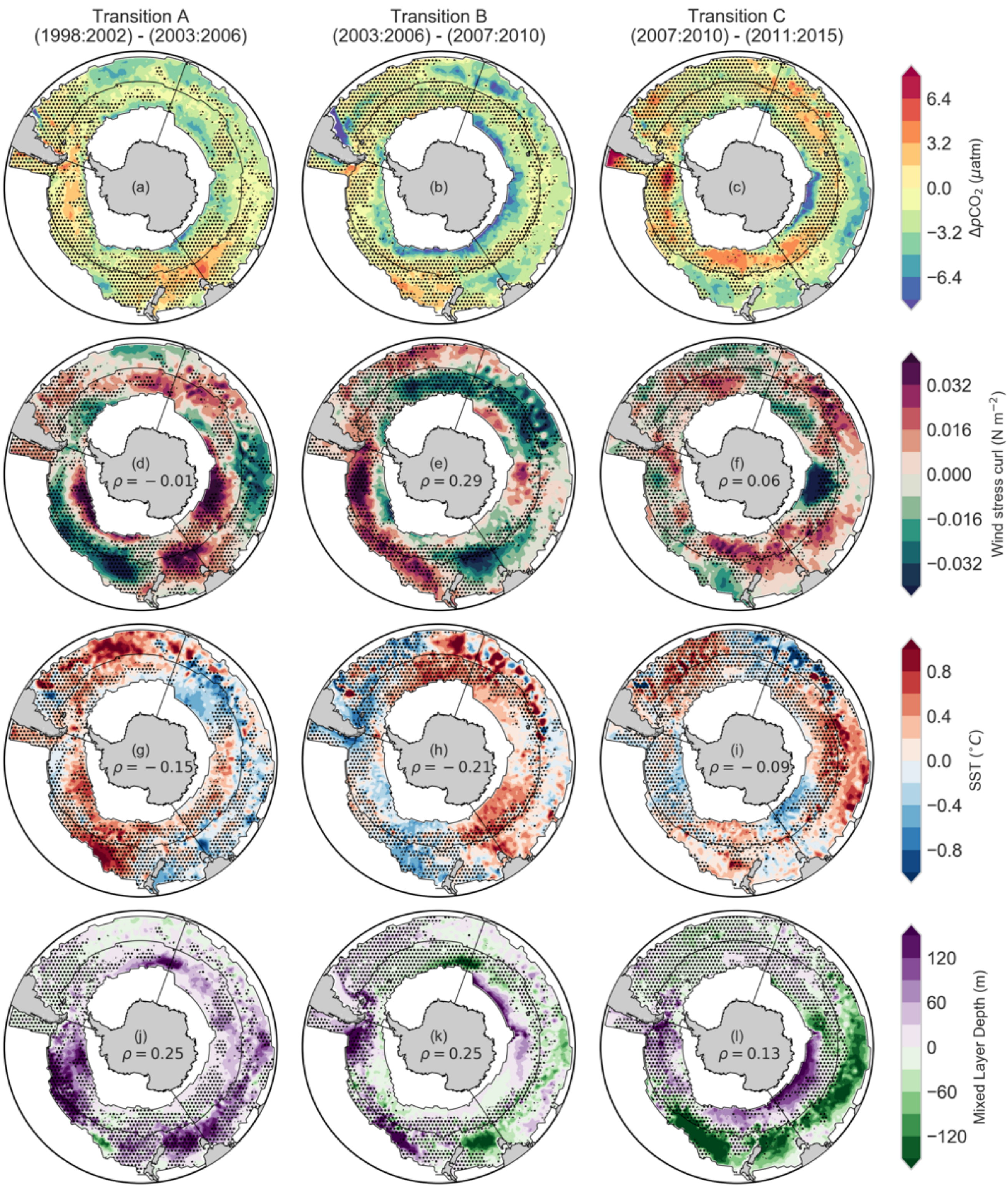

Figure 6: Transitions (relative anomalies) of winter ΔpCO_2 (a-c), wind stress (d-f), sea surface temperature (g-i) and mixed layer depth (j-l) for four periods. The thin black lines show the boundaries for each of the nine regions described by the biomes (Fay and McKinley, 2014a) and basin boundaries. Regions with dots ~~in (a-c)~~ are where ~~the~~ ΔpCO_2 anomalies are not significant ~~ie~~i.e: standard deviation of the anomalies between ~~models is~~methods are greater than the absolute mean of method anomalies, as described in equations ~~S1~~6 to ~~S3~~8.

3.5.1 ~~Wind dominated~~MLD driven interannual variability of pCO_2 in winter

Our results indicate that there is not one dominant driver of ΔpCO_2 interannual transition anomalies in winter. While MLD is on average the stronger driver, its dominance on ΔpCO_2 is only marginal over SST and wind stress (Figure 6). This marginal dominance over the two other drivers is likely due to MLD being a metric that integrates the complex interaction between wind-driven mixing and winter heat loss to the atmosphere, of which SST is a response (De Boyer Montégut et al., 2004; Sallée et al., 2010). Mechanistically, deeper MLDs would result in greater entrainment of DIC-rich deep waters, while shallower MLDs entrain less DIC-rich waters, thus reducing the DIC pool in winter resulting in potentially stronger ΔpCO_2 uptake in the surface ocean (Lenton et al., 2013).

An important point to note is that SST is negatively correlated with ΔpCO_2 in Figures 6g-i. This is contrary to what is expected for solubility-driven changes of pCO_2 (Takahashi et al., 1993). ~~Based on the observations outlined above, we propose that interannual variability of the regional (basin-scale) characteristics of winter wind stress may be the dominant driver of the saturation and reinvigoration periods.~~

~~These findings suggest that increasing or decreasing interannual winter wind stress variability impacts ΔpCO_2 (and thus FCO_2) by driving changes in turbulent mixing that set the magnitudes of winter entrainment. In the transition to and during winter, this mixing is associated with changes in rates of heat loss that drive loss of buoyancy or weaker stratification (Abernathey et al., 2011). Weaker buoyancy facilitates deepening of the MLD, thus entraining DIC-rich deep waters (Abernathey et al., 2011; Lenton et al.,~~ This indicates that SST – a response to underlying variability and trends in winter buoyancy and mixing – is not a driver of ΔpCO_2 changes in most regions of the Southern Ocean. There are some small sub-regions, where SST could drive the ΔpCO_2 trend, such as in the east Pacific sector of the PFZ during Transition B (Figure 6b,h) but they are spatially and temporally limited. Our results suggest that, in winter, a complex interaction of changing wind stress and buoyancy fluxes that influence MLD and entrainment may play a stronger role than thermodynamics in explaining the ΔpCO_2 interannual transitions.

Wind-stress anomalies (Figure 6d-f) do not correlate strongly with pCO_2 anomalies, with the exception of Transition B, when it has the strongest correlation. We propose that this lack of coherence between the two variables may be a result of two compounding points. Firstly, wind stress is the only truly independent driver in the analysis, with SST and MLD both being used as proxies for ΔpCO_2 in each of the products. Secondly, the wind stress shown in Figure 6d-f considers only wind strength, so it does not take into account potential meridional changes in atmospheric circulation. This is the primary hypothesis presented in Landschützer et al. (2015), suggesting that atmospheric circulation became more zonally asymmetric. This induced a southward shift of warmer waters over the Atlantic and Indian sectors, reducing the depth of the MLD. Conversely, in the eastern Pacific cold winds induced colder SST and thus an increase in solubility.

Past studies have related the variability of Southern Ocean ~~2013). Conversely, decreased wind stress and mixing during winter (on seasonal or interannual time scales) reduces the rate of heat loss (represented as warm anomalies in Figure 5). This results in stronger stratification and shallower winter MLD limits entrainment of DIC, which strengthens the CO_2 winter disequilibrium and leads to a stronger CO_2 sink anomaly (Figure 5). These are the mechanisms that we propose result in decreasing or increasing fluxes with interannual and basin- scale changes in wind stress.~~

~~We propose the link between spatial changes in wind stress and uptake of CO_2 as an alternative hypothesis to temperature being a driver as suggested by Landschützer et al. (2015). Typically an increase in ocean temperature, which reduces CO_2 solubility, results in an increase in ΔpCO_2 (Takahashi et al., 1993). However, seasonal – regional analysis shows that the observed relationship between pCO_2 and SST is counterintuitive (Figure 5a-c,g-i). On this basis we propose that SST is not a driver of pCO_2 in winter. We suggest that this relationship is a product of weaker mixing and Ekman transport that allows warmer waters to shift southward. This also has the impact of strengthening buoyancy that would otherwise bring CO_2 to the surface. In summary, our results suggest that, like pCO_2, the SST changes are also a response to the wind stress and not in themselves the drivers of pCO_2 changes.~~

~~Given the hypothesis that~~ wind stress ~~is the dominant driver of interannual – decadal ΔpCO_2 in winter, it is of interest to understand its potential mechanisms. Past studies have used the~~ to the SAM ~~as a proxy for wind stress variability over the Southern Ocean~~, where the multi-decadal increasing trend has been cited as a reason for the saturation in the ~~1990's~~1990s (Marshall, 2003; Le Quéré et al., 2007; Lenton and Matear, 2007; Lovenduski et al., 2008). ~~While Landschützer et al. (2016) identified the SAM as being a driver of global CO_2 variability, the index does not explain the reinvigoration of the Southern Ocean CO_2 sink in the 2000s.~~ The SAM is often represented as a zonally integrating index (Marshall, 2003), but more recent studies have shown that the SAM, as the first empirical mode of atmospheric variability, is zonally asymmetric (Fogt et al., 2012). The zonal asymmetry of the SAM is thought to be linked with the El Niño – Southern Oscillation and is strongest in winter, particularly over the Pacific sector of the Southern Ocean during a positive phase, ~~thus~~ in accord with the dipole nature of the Pacific–Indian winter wind~~-~~-stress ~~dipole~~transition observed in Figures ~~5d~~6d,e (Barnes and Hartmann, 2010; Fogt et al., 2012). Fogt et al. (2012) noted that the SAM has become more zonally symmetric in summer since the ~~1980's~~1980s, matching the characteristics of the anomalies of wind~~-~~-stress ~~anomalies~~transitions seen in Figure 6d-f~~.~~ and the hypothesis of Landschützer et al. (2015).

~~In summary, we propose that interannual variability of wind stress and its regional expression in winter is the dominant interannual driver of $\Delta p CO_2$ variability in the Southern Ocean. The interannual variability of wind stress is linked to the SAM, but this relationship is nuanced by the zonally (regional) asymmetric variability of the SAM as observed by zonal asymmetry of wind stress in the Pacific and Indian sectors of the Southern Ocean.~~

In summary, our analysis of the drivers of $\Delta p CO_2$ is consistent with the atmospheric asymmetry (dipole) conceptual model associated with the SAM proposed by Landschützer et al. (2015). However, our results suggest that interannual $\Delta p CO_2$ trends are explained by DIC dynamics rather than by the thermodynamic response of pCO_2. A key part of this emphasis on DIC is that our results indicate that $\Delta p CO_2$ and SST are not correlated in a way that supports a thermodynamic control of $\Delta p CO_2$. The reasons for these differences are not clear at this stage, but they could include differences in the temporal resolution of the two studies: the resolution of the seasonal extremes in this study (seasonal modes) vs annual mean in Landschützer et al. (2015).

3.6 Anomalies of $\Delta p CO_2$ and its summer drivers

~~The most marked difference between the summer and winter anomalies, is that $\Delta p CO_2$ (Figures 6a-c) does not correlate with wind stress (Figures 6d-f), thus ruling out wind as a first order driver of summer CO_2. Rather, $\Delta p CO_2$ has the strongest coherence with Chl-*a* (an inverse relationship), which suggests that primary production may be a first order driver of the observed $\Delta p CO_2$ variability. Another difference between summer and winter is that the magnitudes of the transition anomalies are much larger in summer, and thus there are larger regions of significant anomalies (Figure 6a-c).~~

~~Looking more specifically at the significant variability of $\Delta p CO_2$, transition A~~ Compared to the winter transitions, summer transitions (Figure 7) have larger areas where the anomalies between products are within the bounds of the uncertainty. This may be due to the larger magnitude of the anomalies in summer compared to winter (Figure 6). In summer we also see that Chl-*a* (Figures 7j-l) is likely the first-order driver with the highest correlation scores for transitions A and B.

Transition A (P2 – P1 in Figure ~~6a~~7a) is marked by a decrease of CO_2 in the SAZ (Tasman shelf region), ~~mirrored by~~ coinciding with an increase in Chl-*a*. ~~The Atlantic and Indian sectors of the PFZ remain mostly neutral/weak sources marked by a~~ The Drake Passage region experiences a strong reduction of $\Delta p CO_2$ in ~~phytoplankton biomass (Figure 6j).~~ the PFZ, as found by Munro et al. (2015) and Landschützer et al. (2015). Unlike in the Tasman basin, this reduction of $\Delta p CO_2$ is not accompanied by a strong increase in Chl-*a*, but rather a reduction of wind stress and an increase in SST. This is contrary to the annually integrated analysis of Landschützer et al. (2015), who found that cooling drove a reduction of pCO_2 in the eastern Pacific sector of the PFZ. This difference likely arises from the integration of seasons and a longer period (2002–2011) compared to the framework used in this study. In the Indian sector of the PFZ the products agree on a weak increase in ΔpCO_2 corresponding with a weak reduction of Chl-*a*.

Transition B (P3 – P2 in Figure ~~6b),~~7b) shows ~~invigoration of CO_2 uptake in the Atlantic sector of the SAZ and PFZ; and in parts of the Pacific Ocean. Once again, the~~ a large reduction of ΔpCO_2 ~~correlates well with Chl-*a* increases. In~~ in the Atlantic sector of the PFZ and southern SAZ. The reduction coincides with an increase in Chl-*a* and SST in the same region, in agreement with Landschützer et al. (2015).

In transition C (P4 – P3 in Figure ~~6c~~7c) the reduction of the ΔpCO_2 is widespread in the Indian and Pacific Oceans in ~~all three~~both biomes, as the increase in Chl-*a* is similarly widespread~~.~~; however, the increase in Chl-*a* in the Indian sector of the SAZ is not strong compared to other regions where ΔpCO_2 and Chl-*a* variability correspond. Conversely, there is a reduction in Chl-*a* and concomitant increase in ΔpCO_2 along the Polar front in the Atlantic sector, coinciding with the position of the Antarctic Circumpolar Current (ACC~~, which has~~) – a region with high eddy kinetic energy (EKE) (Meredith, 2016). ~~These examples demonstrate~~

Based on these cases we suggest that ΔpCO_2 is driven primarily by Chl-*a* in ~~summer. However, understanding~~regions with high Chl-*a* concentrations. Note that we will not try to explain Chl-*a* variability, which is ~~more~~ complex due to the multitude of factors influencing phytoplankton growth (Thomalla et al., 2011). ~~as there is seemingly no set rule between Chl-*a*,~~ We further suggest that in regions of low Chl-*a*, buoyancy forcing and mixing are higher-order drivers. As suggested for winter variability, these two mechanisms are a complex interaction of variables of which SST and wind stress ~~(Thomalla~~are a part (Abernathy et al., 2011).

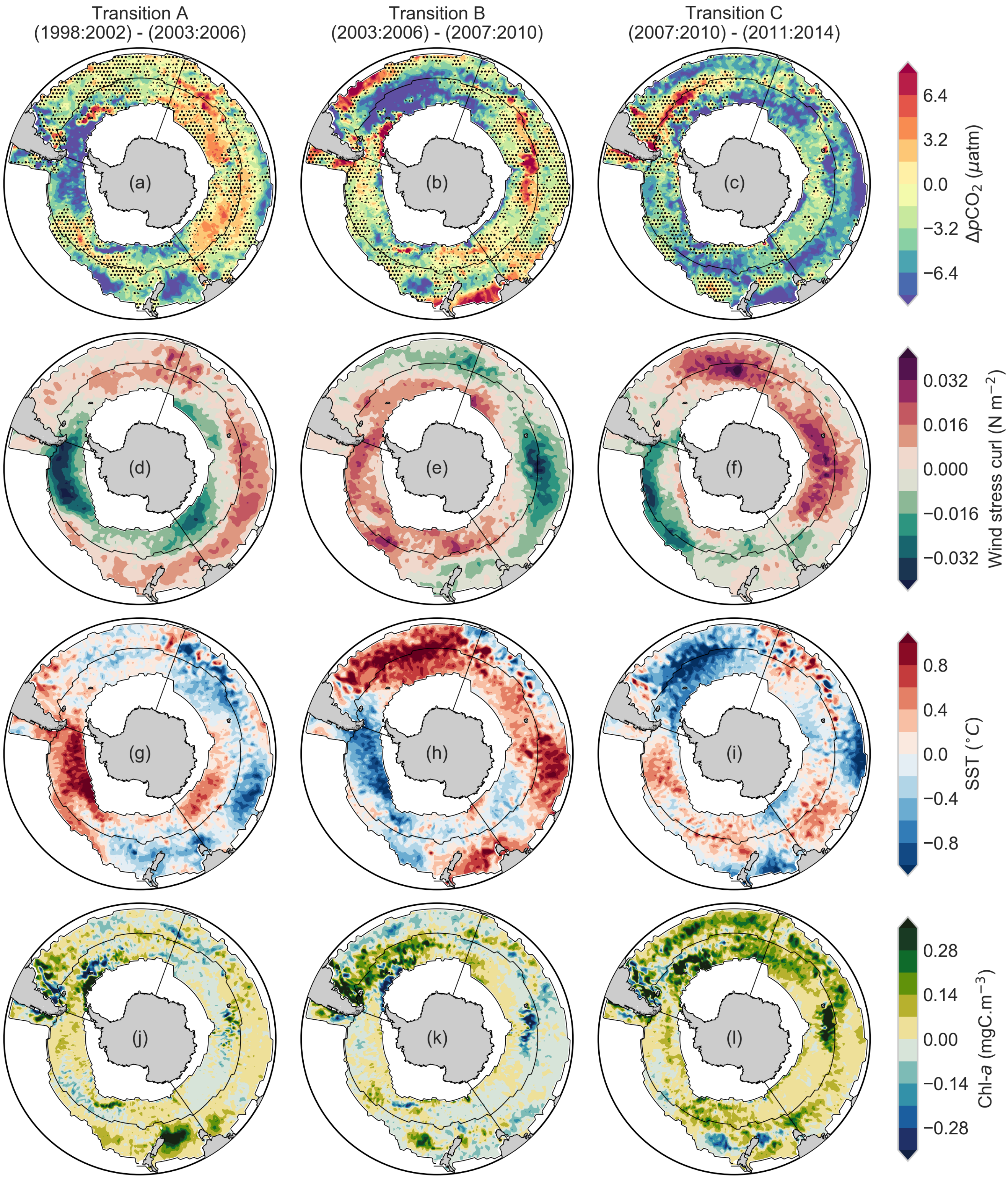
Transition A
(1998:2002) - (2003:2006)
Transition B
(2003:2006) - (2007:2010)
Transition C
(2007:2010) - (2011:2014)
(a)
(b)
(c)
6.4
3.2
0.0
−3.2
−6.4
ΔpCO2 (μatm)
(d)
(e)
(f)
0.032
0.016
0.000
−0.016
−0.032
Wind stress curl (N m−2)
(g)
(h)
(i)
0.8
0.4
0.0
−0.4
−0.8
SST (°C)
(j)
(k)
(l)
0.28
0.14
0.00
−0.14
−0.28
Chl-a (mgC.m−3)

615

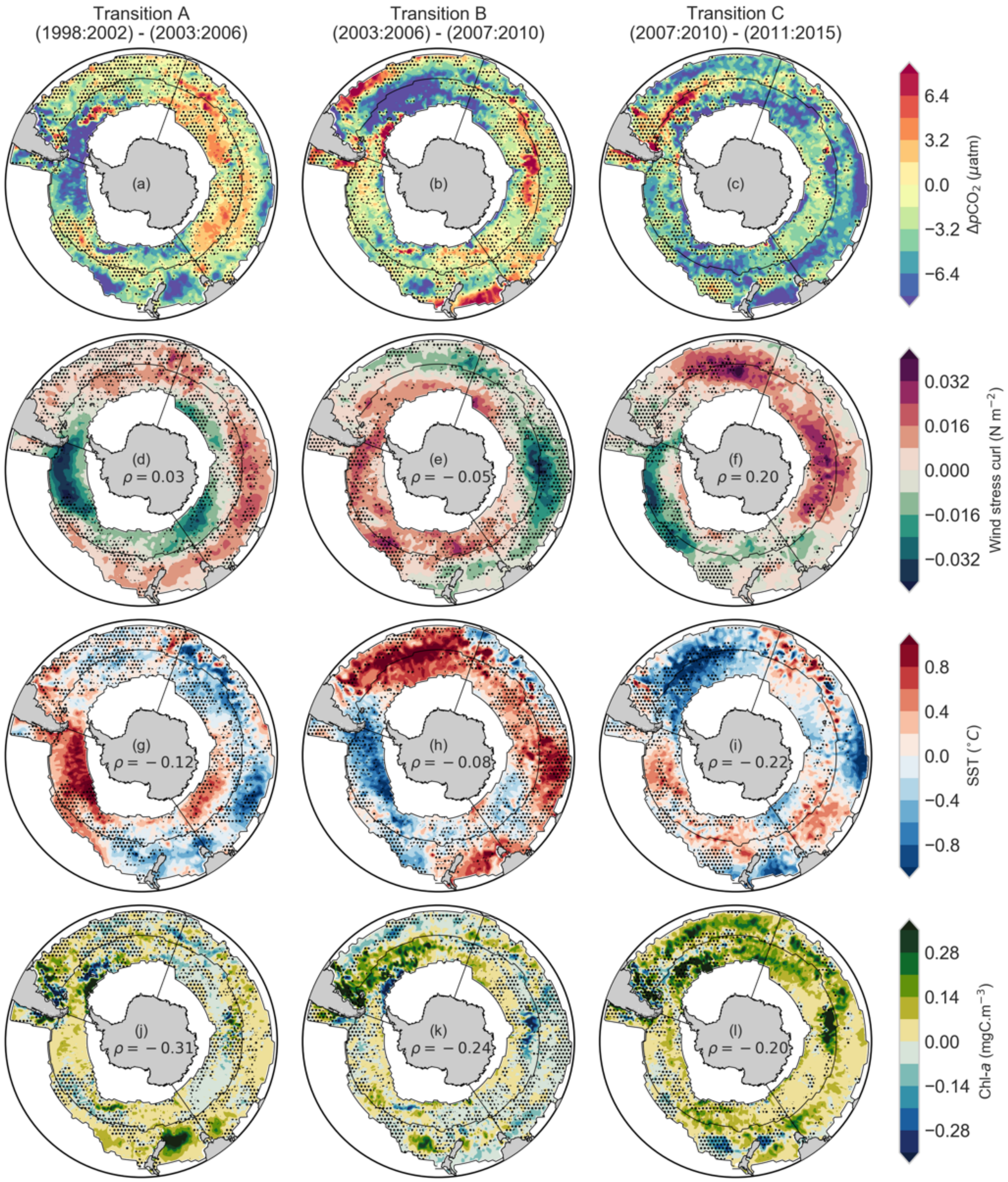

Figure ~~6~~7: Relative anomalies of summer ΔpCO$_2$ (a-c), wind stress (d-f), sea surface temperature (g-i) and mixed-~~-~~layer depth (j-l) for four periods (as shown above each column). The thin black lines show the boundaries for each of the nine regions described by the biomes (Fay and McKinley, 2014a) and basin boundaries. Regions with dots are where ΔpCO$_2$ anomalies are not significant i.e: standard deviation of the anomalies between methods are greater than the absolute mean of method anomalies, as described in equations 6 to 7.

~~There are regions in the Southern Ocean where summer Chl-*a* variability does not coincide with ΔpCO$_2$ variability, particularly in the Indian and Pacific sectors of the SAZ (Figures 6a-c and 6j-l). This may be due to low chlorophyll concentrations, and anomalies thereof, in these regions~~ This then raises the importance of the magnitudes of the interannual variability of ΔpCO$_2$ and its drivers. ~~(Thomalla et al.,~~

~~2011). As a result the other variables, SST and wind stress, may be higher order drivers in low chlorophyll regions, as found by Landschützer et al. (2015) and Munro et al. (2015).~~

~~It is thus important to understand the variability of SST and wind stress in summer. Large SST anomalies between the western Atlantic and eastern Pacific sectors vary as a zonally asymmetric dipole. As in winter, there is a summer wind stress anomaly dipole, but rather than being zonally asymmetric (*e.g.* Pacific Indian), the dipole has annular, north-south variability (Figures 5,6d-f). We suggest that these dipoles in the variability may indicate that the Southern Ocean, as a system, transitions between different states forced by atmospheric variability (Landschützer et al., 2015).~~

~~An important note is that the magnitudes of $\Delta p CO_2$ and its drivers have different magnitudes seasonally.~~ For example, the anomalies of $\Delta p CO_2$ and SST are larger in summer than in winter. Conversely, the wind -stress anomalies are larger for winter than in summer. This is an important consideration for analyses that aim to understand the driving mechanisms, where annual averaging would ~~make it difficult to decompose the true drivers of change.~~weight seasonally asymmetric responses of $\Delta p CO_2$ and its drivers unequally.

3.6.1 Chlorophyll dominated interannual anomalies of pCO_2 in summer

Our finding that Chl-*a* is the dominant driver of interannual $\Delta p CO_2$ variability should not be surprising given that models and observations support this notion (Hoppema et al., 1999; Bakker et al., 2008; Mahadevan et al., 2011; Wang et al., 2012; Hauck et al., 2013; 2015; Shetye et al., 2015). However, our data show that the dominance of interannual Chl-*a* variability over $\Delta p CO_2$ is largely limited to regions where Chl-*a* is high, such as the Atlantic, the Agulhas retroflection and south of Australia and New Zealand (Figure ~~7~~8).

The spatial variability of high Chl-*a* regions in the Southern Ocean is complex due to the dynamics of light and iron limitation (Arrigo et al., 2008; Boyd and Ellwood, 2010; Thomalla et al., 2011; Tagliabue et al., 2014; 2017). This complexity is highlighted in Thomalla et al. (2011), where the Chl-*a* is characterized into regions of concentration and seasonal cycle reproducibility (Figure ~~7~~8). The seasonal cycle reproducibility (SCR) is calculated as the correlation between the mean annual seasonal cycle and the observed chlorophyll time series. Here we use the approach of Thomalla et al. (2011), in Figure ~~7~~8, as a conceptual framework to understand the interannual variability of $\Delta p CO_2$.

3.6.2 High chlorophyll regions

While regions of high SCR (dark green in Figure ~~7~~8) do not correspond with the interannual variability of Chl-*a* (Figure ~~6j~~7j-l), the framework by Thomalla et al. (2011) does present a hypothesis by which the variability of Chl-*a* and its drivers can be interpreted. This is, that the variability of Chl-*a* in a region is a complex interaction of the response of the underlying physics (mixing vs~~.~~ buoyancy forcing~~)~~,, which modulate light ~~(~~via ~~the~~ MLD~~)~~ and iron supply~~,~~) to the interannual variability in the drivers (SST and wind stress). This complexity is exemplified by strong warming in the Atlantic during transition B, which results in both an increase and decrease in Chl-*a*, with inverse consequences for $\Delta p CO_2$. The effect is ~~an~~ even stronger in transition C, where strong cooling in the Atlantic results in both a decrease and increase of Chl-*a* (Figure ~~6i~~7i,l). In both transition A and B, the respective increase and decrease of Chl-*a* occur roughly over the ACC, while the opposing effects during transitions A and B occur roughly to the north and south of the ACC region. These temperature changes may impact the stratification of the region, but complex interaction with the underlying physics results in variable changes in Chl-*a*.

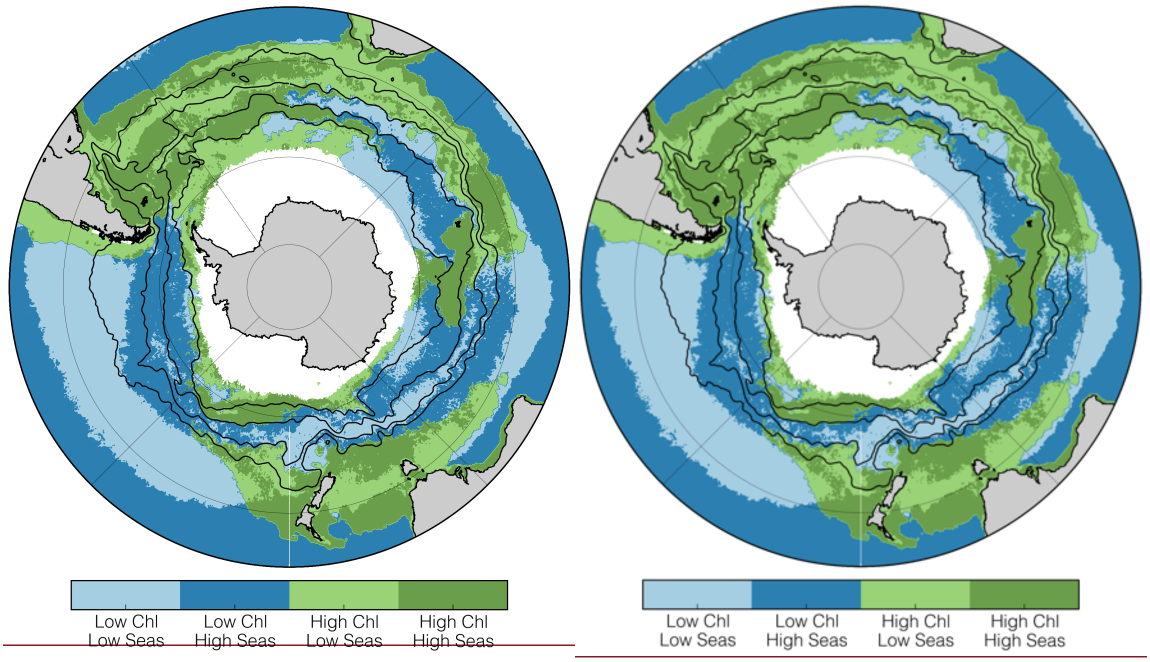

Figure ~~9~~8: Chl-*a* seasonal cycle reproducibility and iron-supply mechanisms in the Southern Ocean ~~(a)~~. Regions of chlorophyll biomass and seasonal cycle reproducibility from Thomalla et al. (2011) (using SeaWIFS data). Seasonality is calculated as the correlation between the mean annual seasonal cycle compared to the observed chlorophyll time series. A correlation threshold of 0.4 ~~was~~is applied to each time series to distinguish between regions of high and low seasonality; similarly, a threshold of 0.25 mg m^{-3} ~~was~~is used to distinguish between low or high chlorophyll waters. Black lines ~~show~~showing the ~~Southern Ocean~~ fronts are calculated ~~by sea surface height (~~using altimetry thresholds from Swart et al~~.,~~. (2010).

It is clear that, while there is a relationship between Chl-*a* and pCO_2 as well as a relationship between wind stress and SST in summer, the relationship between wind forcing, Chl-*a* and pCO_2 is not as strong as in the winter anomalies (Figure ~~5~~6). It may be that enhanced summer buoyancy forcing resulting from summer warming and mixed layer eddies drives a more complex response to wind stress in the form of vertical velocities and mixing, which influence the iron supply and the depth of mixing ~~depth~~ (McGillicuddy, 2016; Mahadevan et al., 2012).

Mesoscale and ~~sub-mesoscale~~submesoscale processes may have a part to play in these dynamic responses of Chl-*a* to changes in SST and wind stress (amongst other drivers). For example, eddy-driven slumping could act to ~~rapidly~~ shoal the mixed layer rapidly (Mahadevan et al., 2012; Swart et al., 2015b; du Plessis et al., 2017). This allows phytoplankton to remain within the euphotic zone and thus ~~grow (while~~ensuring growth as long as iron is not limiting~~)~~.. Similarly, Nicholson et al. (2016) and Whitt et al. (2017) demonstrated that submesoscale processes could supply iron to the mixed layer by submesoscale mixing. Importantly, these mechanisms rely on a mixing transition layer that has sufficient iron ~~that is able~~ to sustain growth~~. Weak~~ – weak dissolved iron gradients in the Pacific and east Indian sectors of the Southern Ocean could explain the lack of phytoplankton in these regions (Tagliabue et al., 2014; Nicholson et al., 2016). Much of the spatial character of the transition anomalies occurs at mesoscale, which strengthens the view that these mesoscale and ~~sub-mesoscale~~submesoscale processes may be key to ~~explain~~explaining changes in Chl-*a* (Figure ~~6j~~7j-l).

3.6.3 Low chlorophyll regions

Entrainment and stratification can explain much of the variability in the eastern Pacific and Indian sector of the PFZ (with the exception of the wake of the Kerguelen Plateau). For example, in the eastern Pacific in transition A (Figure ~~6a~~7a,d,g), strong warming and weaker winds have little impact on Chl-*a*, but a decrease in $\Delta p CO_2$ is observed. Conversely, cooling in the west Indian sector of the PFZ results in a weak increase in $\Delta p CO_2$ during the same transition. In both these cases, the effect of cooling or warming on $\Delta p CO_2$ is negligible relative to the impact of entrainment or stratification respectively. The effect is reversed in the eastern Pacific during transition B, where strong cooling results in a weak reduction of $\Delta p CO_2$ rather than the increase that would be expected from entrainment. This is the mechanism that Landschützer et al. (2015) ascribed to the reduction of $\Delta p CO_2$ in the Pacific, but the effect observed in ~~Figure~~ 6b is weak.

In summary, regions with high~~-~~-biomass Chl-*a* ~~integrates~~integrate the complex interactions between SST, wind stress, MLD and ~~sub-mesoscale~~submesoscale variability, resulting in large interannual $p CO_2$ variability compared to low~~-~~-biomass regions~~. In low Chl-*a* regions,~~, where wind~~-~~-driven entrainment~~/~~ and stratification are more likely drivers of $\Delta p CO_2$.

4 Synthesis

In this study, an ensemble mean of empirically estimated $\Delta p CO_2$ is used to investigate the trends and the drivers of these trends in the Southern Ocean. The estimated $\Delta p CO_2$ shows that the seasonal cycle is the dominant mode of variability imposed upon weaker interannual variability. The ~~data~~ensemble estimates are separated into domains defined by functional biomes and oceanic basins to account for the roughly basin~~-~~-scale zonal asymmetry observed in preliminary analyses of $\Delta p CO_2$ (Fay and McKinley, 2014a). A seasonal ~~decomposition~~framework is applied to the domains, revealing that winter and summer variability is decoupled for each region. The increase and subsequent decrease of $p CO_2$ (and air-sea CO_2 fluxes) is in accordance with recent studies showing a saturation of the Southern Ocean CO_2 sink in the ~~1990's~~1990s, followed by the reinvigoration in the ~~2000's~~2000s (Le Quéré et al., 2007; Landschützer et al., 2015).

While there is agreement around the mean of the ensemble, there is a large amount of uncertainty around the estimates due to a lack of agreement between products on a regional level. This uncertainty likely stems from the way that each method interpolates sparse winter data (Rödenbeck et al., 2015; Gregor et al., 2017). We thus interpret only regions where the three empirical products are in agreement.

We suggest that changes in the characteristics of the seasonal cycle of the drivers of $p$$CO_2$ define the interannual variability of $p$$CO_2$. In other words, the mechanisms that drive interannual modes of variability are embedded in the seasonal cycle.

~~We~~Using this approach, we propose a refinement on the hypothesis put forward by Landschützer et al. (2015) by adding a seasonal constraint. The authors posit that $\Delta p$$CO_2$ variability is driven by changes in atmospheric circulation that in turn affect advection of water masses, thus impacting stratification. Our results also show that winter $\Delta p$$CO_2$ variability is ~~driven primarily by changes in winter wind stress~~best correlated with MLD, which ~~influences the resulting convective~~indicates that entrainment of deep DIC-rich water masses is an important mechanism of $\Delta p$$CO_2$ variability (Lenton et al., 2009; 2013~~). This winter~~; Landschützer et al., 2015). The inverse relationship between SST and $\Delta p$$CO_2$ also suggests that in most cases $\Delta p$$CO_2$ is not thermodynamically controlled. Winter $\Delta p$$CO_2$ variability has a longer mode than summer ~~inter-annual~~ variability~~. We~~, which we attribute ~~this longer winter mode of variability~~ to the decadal-mode variability of the Southern Annular Mode~~, which has a decadal mode~~ (Lovenduski et al., 2008; Fogt et al., 2012; Landschützer et al., 2016). This mechanism is likely dominant in winter due to its role in large seasonal net heat losses that drive convective overturning of the water column.

We suggest that interannual summer variability of $\Delta p$$CO_2$ occurs from a baseline set by an interannual winter trend. Moreover, the shorter time-scale summer interannual variability of $\Delta p$$CO_2$ (roughly 4 – 6 years) is driven primarily by Chl-*a*. ~~Wind stress~~Buoyancy forcing and ~~sea surface temperature~~mixing still influence $\Delta p$$CO_2$ in summer~~,~~ but are lower~~-~~-order drivers. We propose that the interannual variability of the summer seasonal peak is linked to the complex interaction of mid-latitude storms with the strong mesoscale and ~~sub-mesoscale~~submesoscale gradients in the Southern Ocean.

Overall, we propose that although ~~the~~mechanisms linked to winter wind stress ~~linked mechanisms~~ explain the decadal trends in the strengthening and weakening of CO_2 uptake by the Southern Ocean, summer drivers may explain the ~~inter-annual~~shorter term interannual variability ~~in the decadal trends~~ (Lovenduski et al., 2008; Landschützer et al., 2015).

Lastly, it is important to note that this study can be improved by two factors. Firstly, increasing the ~~ensemble~~length of the time series would allow for the identification of regular seasonal modes of variability. Moreover, the length of the anomaly periods could also then be adjusted to understand variability of the drivers better. Secondly, improving machine~~-~~-learning ~~methods shows~~estimates of pCO$_2$ so that there is ~~still considerable disagreement~~better regional agreement between ~~the different approaches. This is likely driven by the lack of pCO$_2$ measurements~~products would decrease the area of insignificant variability. Rödenbeck et al. (2015) and Ritter et al. (2017) attribute the uncertainty to the individual methods' interpolation of sparse data in the Southern Ocean ~~as found~~. This issue is being addressed by ~~Rödenbeck et al. (2015). Autonomous~~the community with autonomous sampling platforms ~~will likely play a role in~~ closing ~~this~~the "observation gap~~", but~~". However, strategic deployment and sampling strategies will be critical to constrain and improve our understanding of CO$_2$ in the non-stationary context (McNeil and Matear, 2013; Monteiro et al., 2015).

S Supplementary Materials

S1 Wind speed and regional surface area

The regional magnitude of integrated air-sea CO_2 fluxes ~~is~~are in part determined by the wind speed and surface area of the specific region. Figure S1a shows the average wind speeds for summer and winter for each of the regions as defined in Figure 1. The wind product used is CCMP v2 (Atlas et al~~.~~., 2011). Figure S1b shows the surface area of each of the regions. Note that the Indian sector of the PFZ has both the highest average wind speed and has the largest surface area. This explains the dominance of the region in the determination of interannual variability of FCO_2 (Figure ~~S2~~S3), even though ΔpCO_2 (Figure 4) variability is relatively weak.

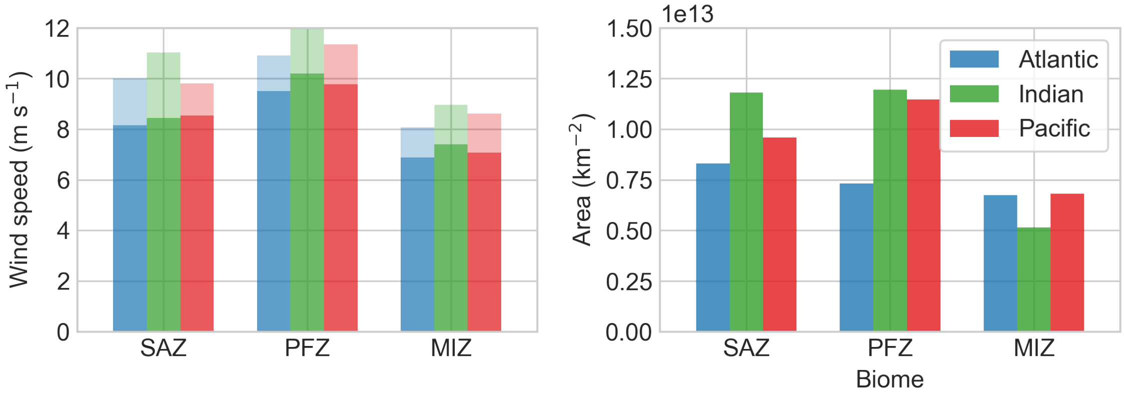

~~(a)~~ ~~(b)~~

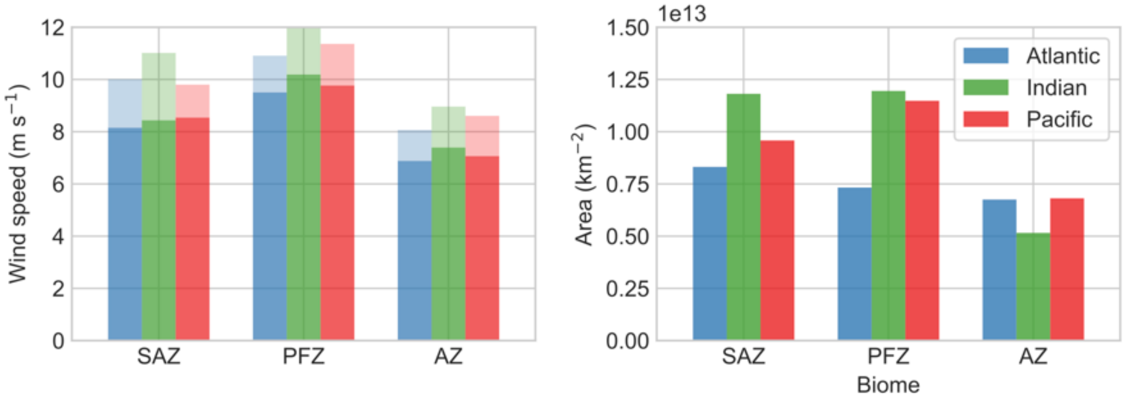

Figure S1: (a) Average wind speeds for each of the biomes for summer (dark) and winter (light). The ocean basins are shown by the colours ~~as shown~~depicted in the key for (b~~). (b)~~), which shows the size of each region separated by biome and basin.

S2 Seasonal time series

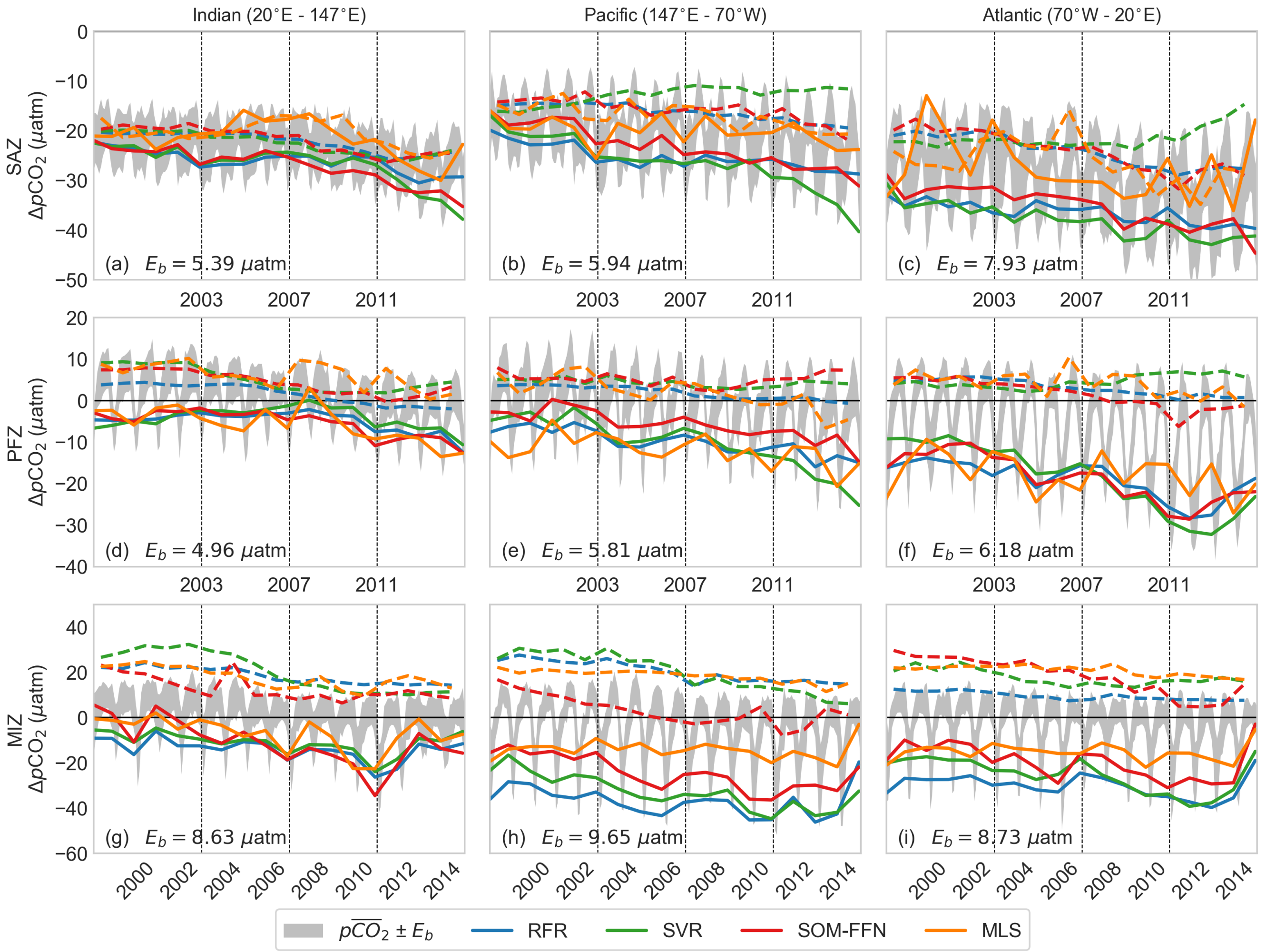

'90

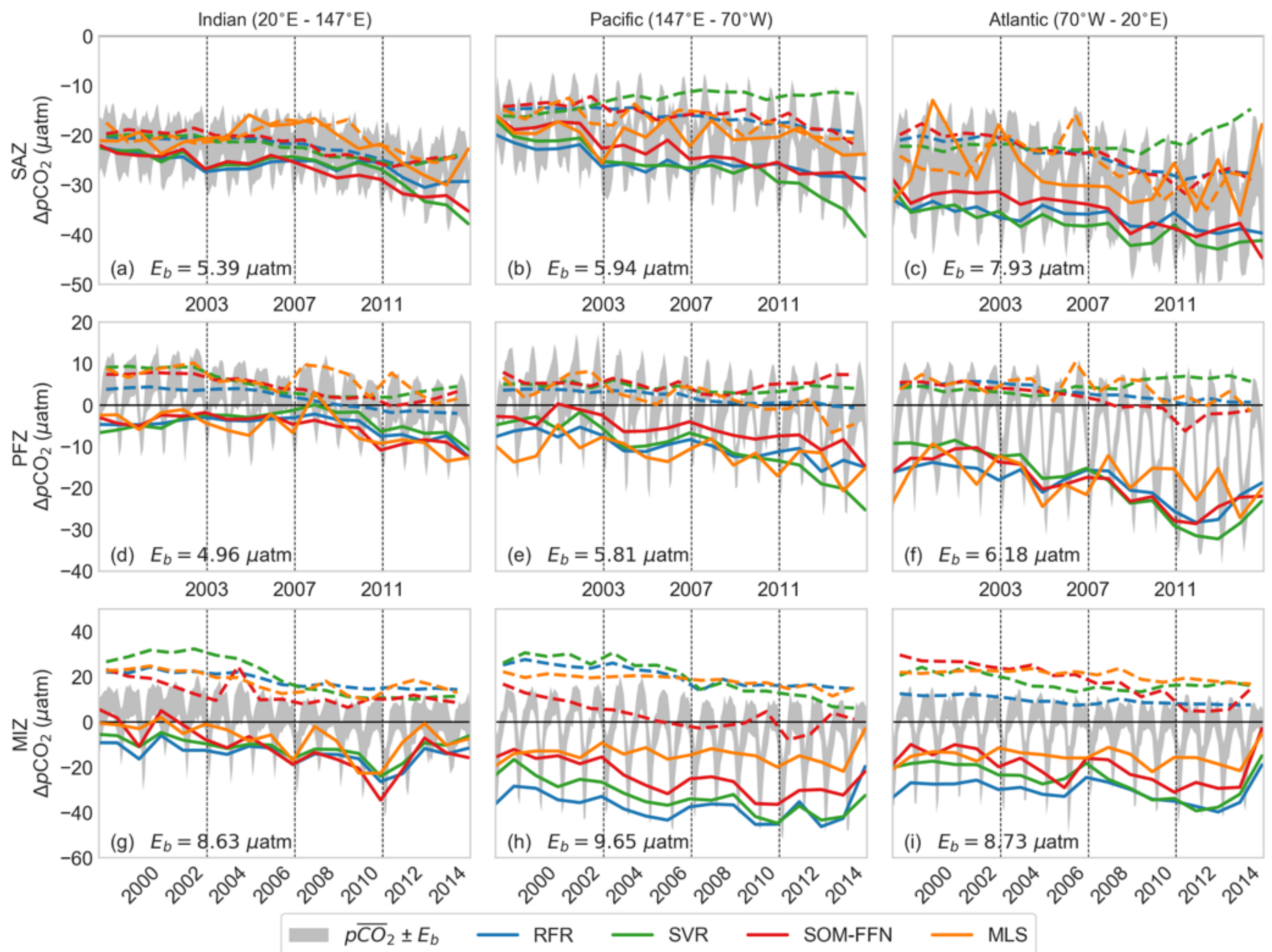

Figure S2: The regional breakdown of the seasonal averages for ΔpCO_2. The seasonal mean for summer (solid) and winter (dashed) for each method is represented by the different coloured lines as shown in the key, where MLS is the Mixed Layer Scheme. The other methods are as in the main text. The grey fill is the ensemble mean $\Delta pCO_2 \pm E_b$, where E_b is the between-method error calculated as in ~~Eq (~~Equation 5~~).~~.

Figure S2 shows the seasonal time series for each region, maintaining separate seasonal averages for each method. We also include the Marginal Ice Zone plots, with all plots showing the average between-method error.

The Mixed Layer Scheme (MLS) method by Rödenbeck et al. (2013) is also included. Note that the MLS is not a machine~~-~~-learning method as it incorporates prior knowledge of the system. The method results in divergent estimates of ΔpCO_2, particularly in the SAZ. The MLS fails to produce a seasonal cycle, with winter and summer ΔpCO_2 having the same magnitude. Further work will have to be done to understand the cause for this difference. We do not include MLS in the main ensemble as we cannot explain this difference. The methods are in much better agreement in the PFZ~~ and MIZ. ~~.

S3 Air-Sea CO_2 Fluxes

Air~~-~~-sea CO_2 fluxes are calculated with:

$$FCO_2 = k_w \cdot K_0 \cdot (p\mathrm{CO}_2^{\mathrm{sea}} - p\mathrm{CO}_2^{\mathrm{atm}}) \quad \text{(S1)}$$

The gas transfer velocity (k_w) is calculated using a quadratic dependency of wind speed with the coefficients of ~~(~~Wanninkhof et al., 2009~~).~~. Coefficients from Weiss (1974) are used to calculate K_0 and $\Delta p\mathrm{CO}_2$ is estimated by the empirical models. Wind speed is calculated from the u and v vectors ($\sqrt{u^2 + v^2}$) of the Cross-Calibrated Multiplatform Product (CCMP) v2 (Atlas et al., 2011; Wentz et al., 2015). Wind speed is one of the largest contributors to the uncertainty in flux estimates, ~~thus~~so the choice of the wind product could have a large impact on flux estimates as well as interpretation of the drivers of CO_2 (Takahashi et al., 2009). We use the ensemble mean $\Delta p\mathrm{CO}_2$ from Figure 4 to calculate fluxes ~~–~~– note that ~~this~~the ensemble mean does not include the MLS shown in Figure S2.

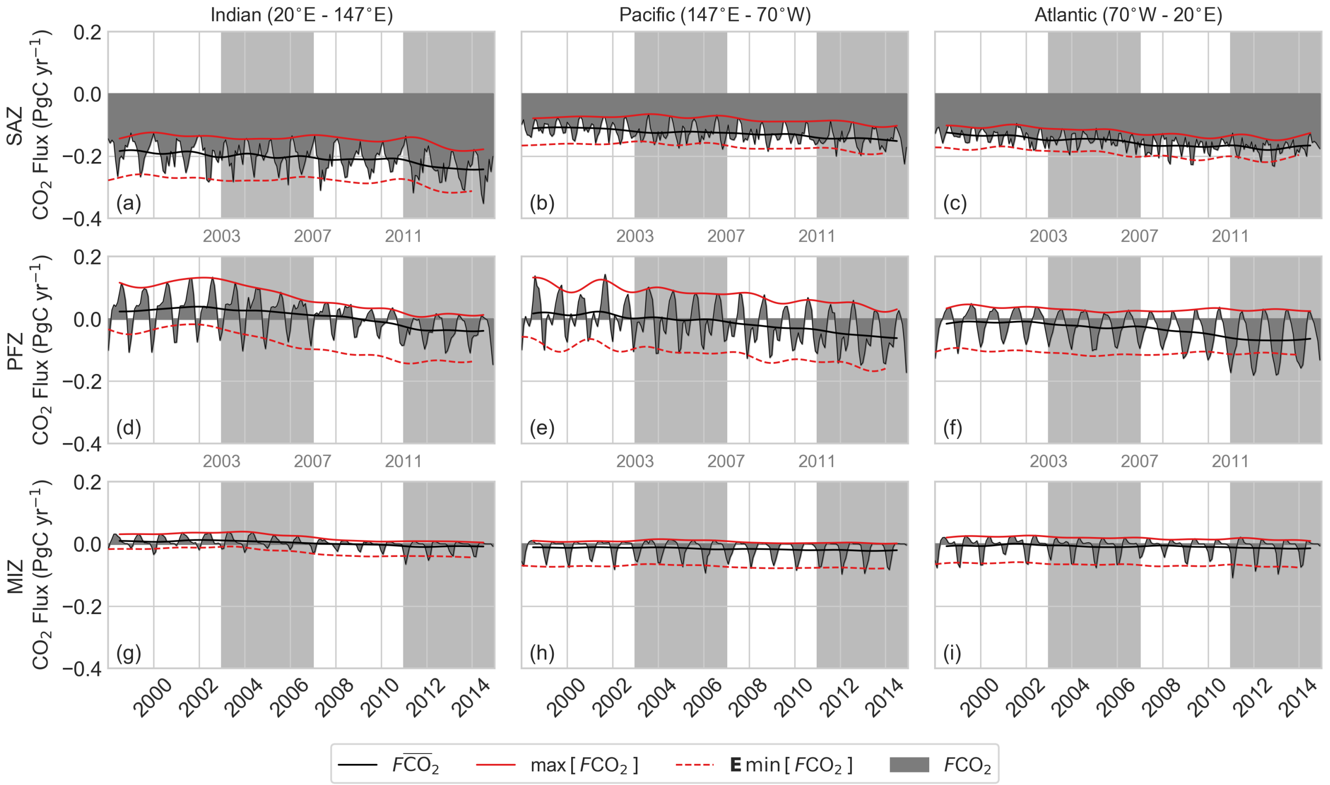

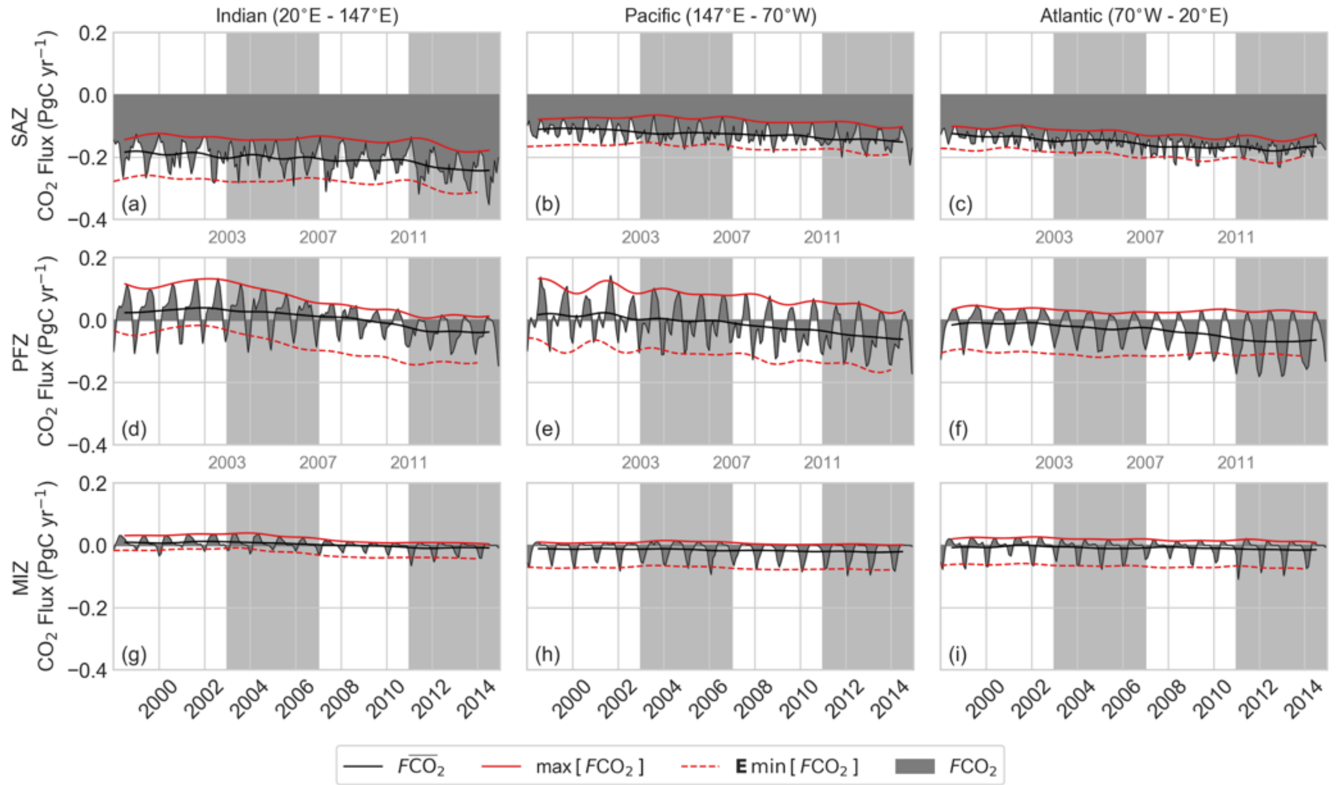

Figure S3: FCO$_2$ (dark grey) plotted by biome (rows) and basin (columns). Biomes are defined by Fay and McKinley (2014a). The solid red line shows the maximum for each year (winter outgassing) and the dashed line shows the same line less the average difference between the minimum and maximum – this is the expected amplitude. Lighter grey shading in (a-i) shows periods used in Figure 5 and 6. Note that fluxes in the MIZ are calculated from a reduced surface area to maintain consistency between methods.

Mean FCO$_2$ is shown in Figure S3. Note that the apparent weak fluxes in the MIZ are due to the reduction of the surface area and ~~thus~~hence flux to maintain equal weighting between machine~~-~~-learning methods. The SAZ clearly dominates the annual uptake of CO$_2$ in the Southern Ocean, but the interannual variability is dominated by the PFZ. An interesting point of the SAZ is that the seasonal cycle of wind speed (strong in winter, weak in summer) opposes that of ΔpCO$_2$ sink (weak in winter, strong in summer). The net result is that, compared to ΔpCO$_2$, the seasonal amplitude of FCO$_2$ is reduced. The same effect shifts the mean flux in the PFZ, but does not affect the amplitude, where outgassing is amplified in winter and the sink is weaker than if wind speed ~~was~~were constant. Lastly, Figures S3a,d show that the Indian sector of the Southern Ocean dominate both uptake (SAZ) and the interannual variability (PFZ).

S4 ~~Uncertainty of the transition anomalies~~

~~The transition anomalies are not calculated from the mean of the three methods. Rather we calculate the anomalies for each individual method with:~~

$$\cancel{a_{n(p')} = \bar{s}_{n(p)} - \bar{s}_{n(p-1)}} \qquad \cancel{\text{(S2)}}$$

~~where s are the estimates for a particular model, n represents an individual model and p represents P1 to P4. The result, $a_{n(p')}$ thus represents the anomaly for two periods for a particular model. We then calculate the average of the anomalies with:~~

$$\cancel{a_{p'} = \frac{1}{N} \cdot \sum_{n=1}^{N} a_{n(p')}} \qquad \cancel{\text{(S3)}}$$

~~where N is 3, the number of models. We then calculate the standard deviation of the three anomalies (e_{p^t}), which is analogous to the between-model error, with:~~

$$\cancel{e_{p^t} = \sqrt{\frac{1}{N} \cdot \sum_{n=1}^{N} \left(a_{n(p^t)} - \overline{a_{n(p^t)}}\right)^2}} \qquad \cancel{(S4)}$$

~~where the terms are consistent with those above. We use e_{p^t} as an uncertainty threshold where anomalies are only considered significant if $|a_{p^t}| > e_{p^t}$. These regions are masked in Figures 5a-c and 6a-c. Figure S4 shows the winter (a-c) and summer (d-f) e_{p^t} for each transition anomaly.~~

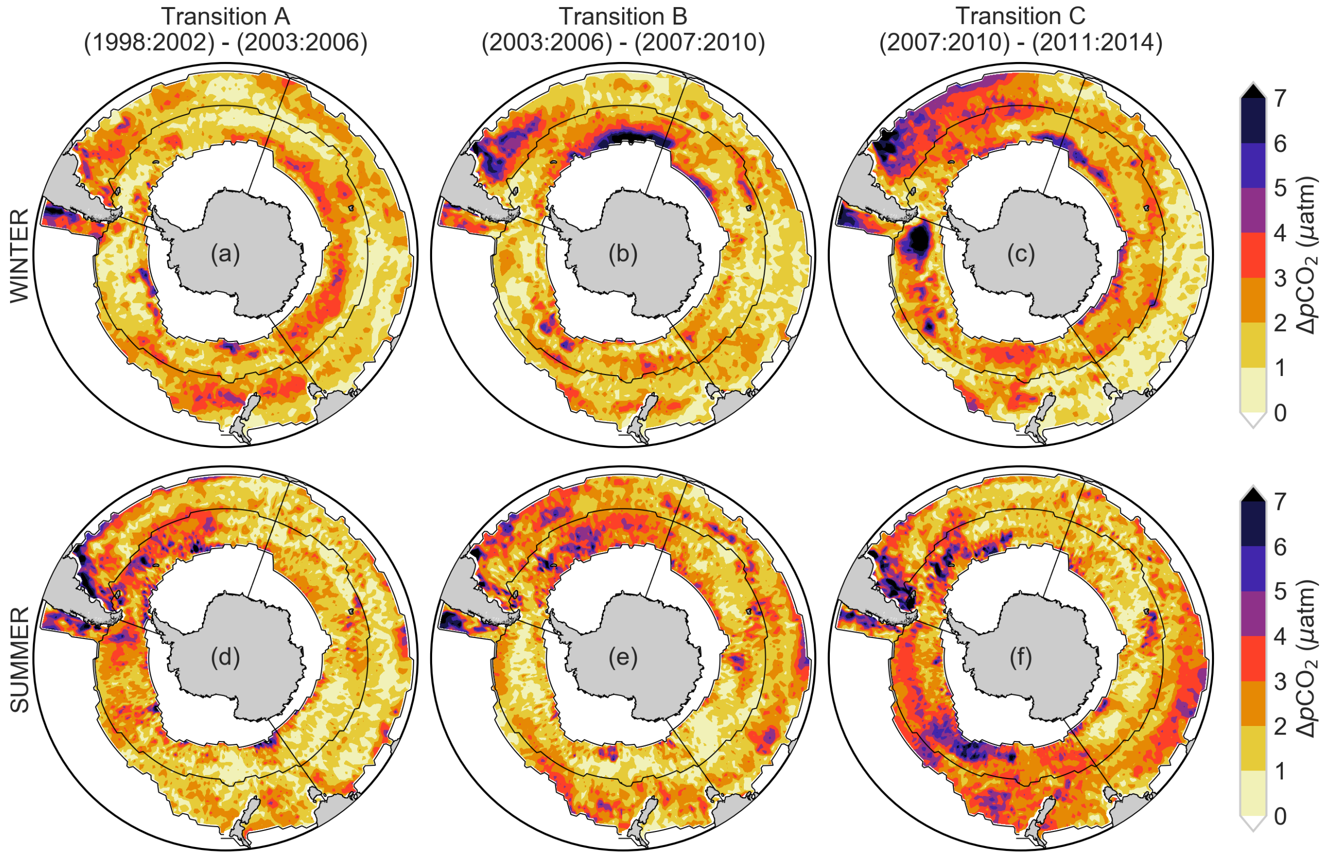

~~**Figure S4: Maps of the standard deviation between empirical methods for the anomalies. These are used as thresholds for ΔpCO_2 in Figures 5(a-c) and 6(a-c) for winter and summer respectively. When the standard deviation exceeds the absolute value average anomaly, the values are masked as shown in Figures 5 and 6.**~~

~~S5~~ Additional driver variables

Here we show additional variables that accompany Figures ~~5~~6 and ~~6~~7. Figure ~~S5~~S4 shows winter Chl-*a*, u- and v-components of wind~~ and~~, while Figure ~~S6~~S5 shows summer MLD, u- and v-components of wind. These variables ~~were~~are not included in the main analyses as they ~~did~~do not contribute significant information to the proxy variables already present (wind stress, SST and MLD/Chl-*a*). It is interesting to note that the u- and v- components of wind speed highlight the zonally asymmetric dipole during winter (Figures ~~S5d~~S4d,e,g,h) and the annular dipole during summer (Figures ~~S6d~~S5d,e).

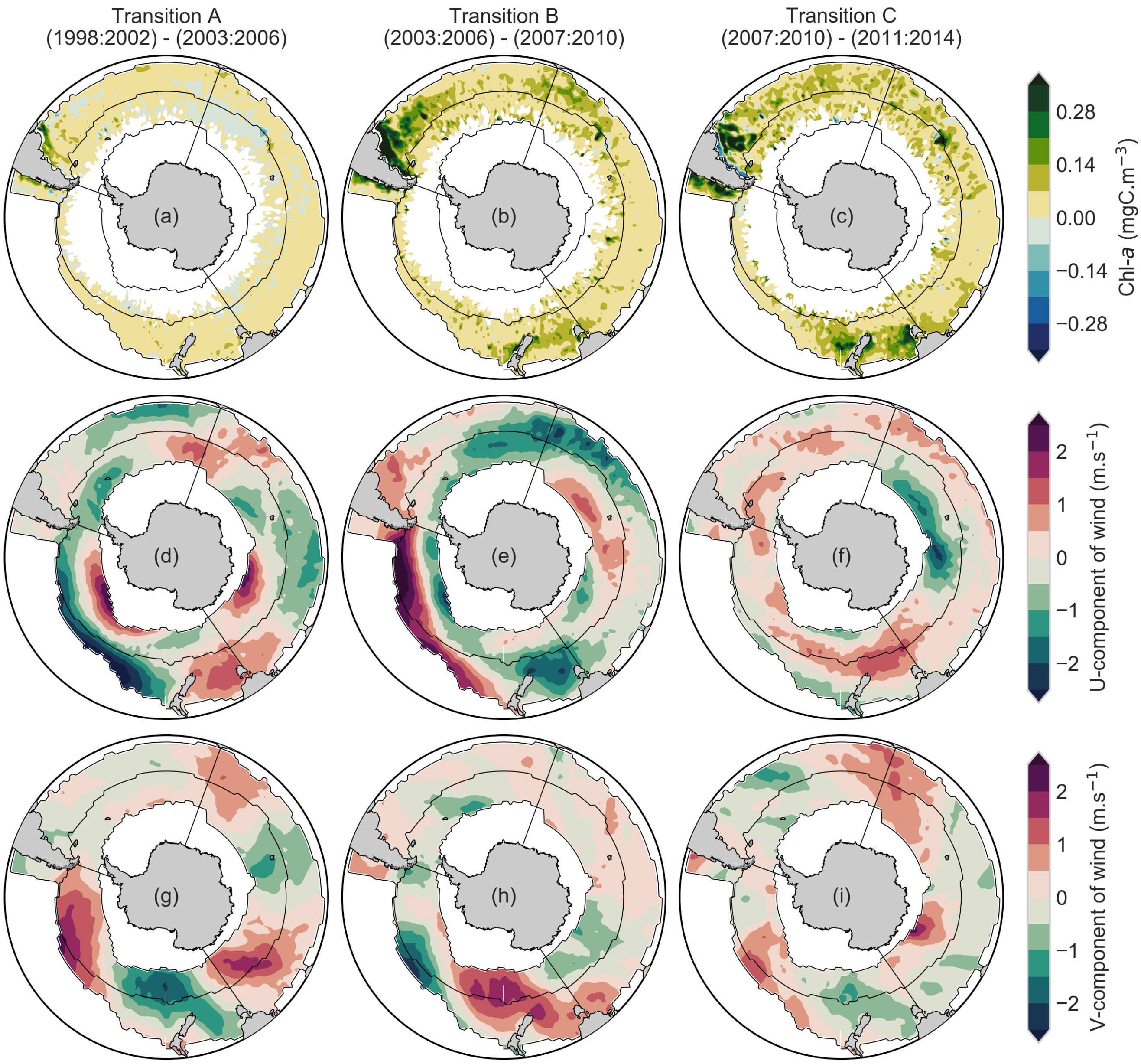

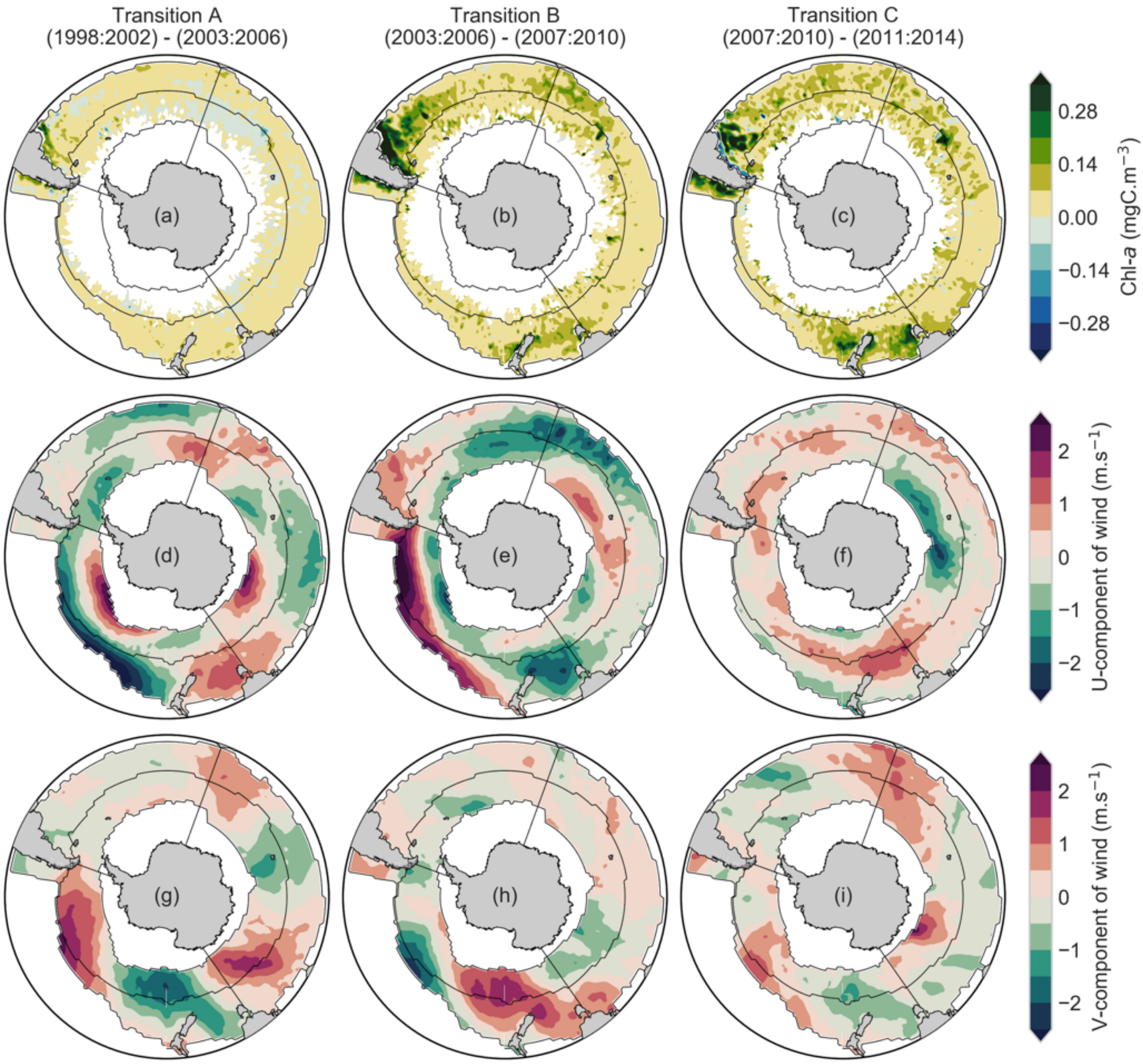

Figure ~~S5~~S4: Relative anomalies of winter ~~chlorophyll~~Chl-*a* (a-c), u- (d-f), and v-components (g-i) of wind for four periods (as shown above each column). The thin black lines show the boundaries for each of the nine regions described by the biomes (Fay and McKinley, 2014a) and basin boundaries.

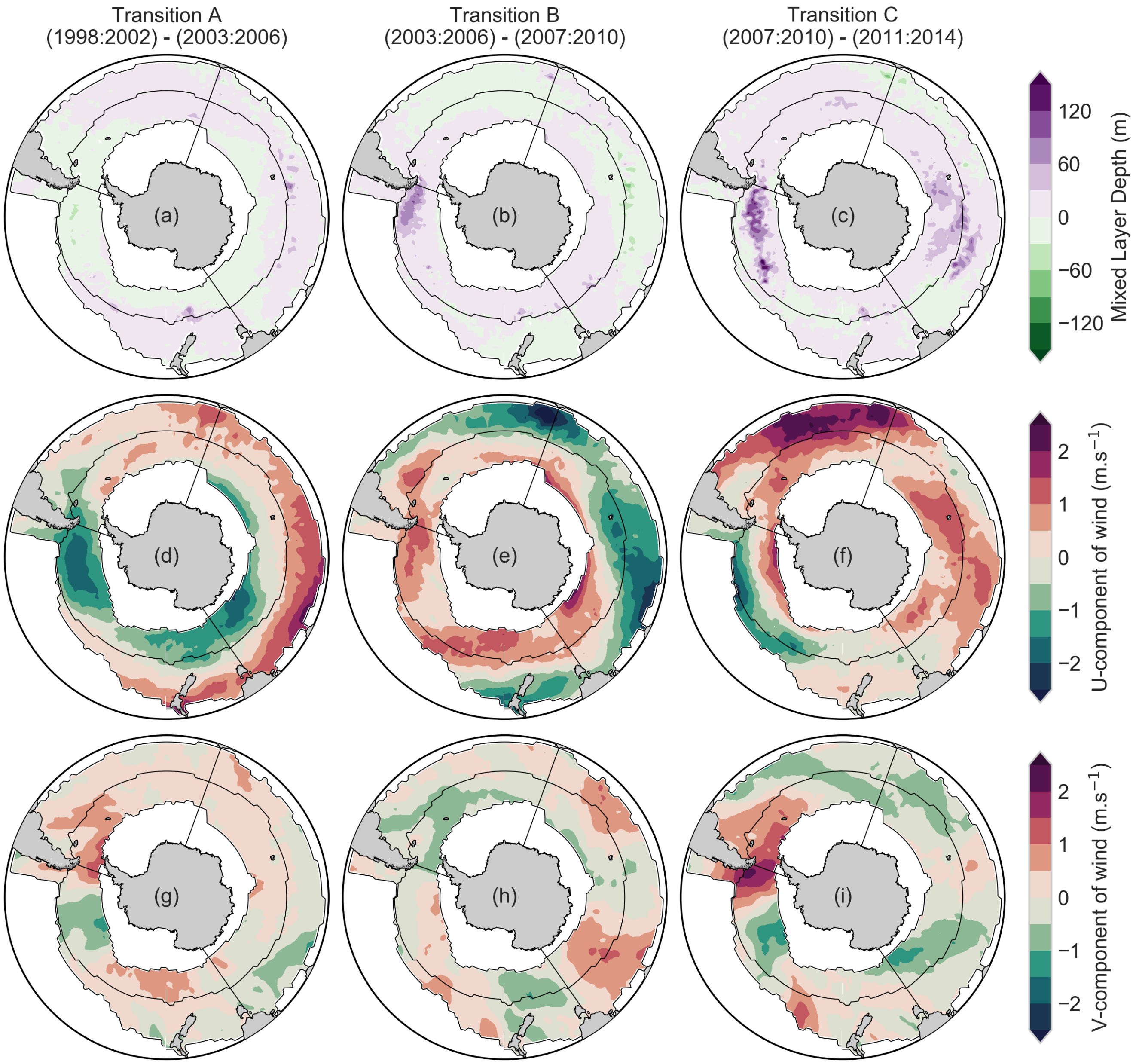

Transition A
(1998:2002) - (2003:2006)
Transition B
(2003:2006) - (2007:2010)
Transition C
(2007:2010) - (2011:2014)
(a)
(b)
(c)
(d)
(e)
(f)
(g)
(h)
(i)
Mixed Layer Depth (m)
120
60
0
−60
−120
U-component of wind (m.s−1)
V-component of wind (m.s−1)
2
1
0
−1
−2

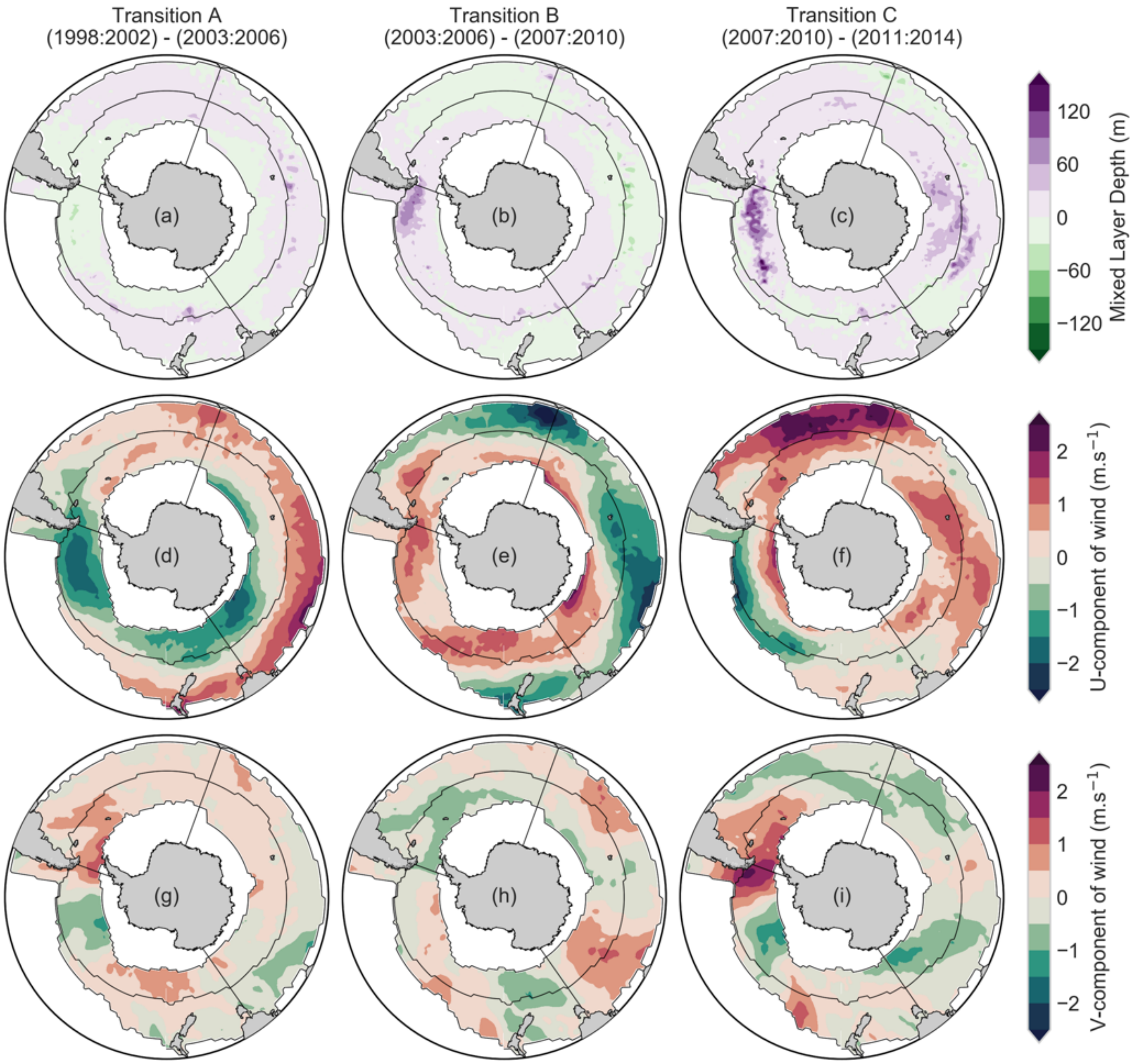

Figure ~~S6~~S5: Relative anomalies of summer mixed layer depth (a-c), u- (d-f), and v-components (g-i) of wind for four periods (as shown above each column~~)..~~). The thin black lines show the boundaries for each of the nine regions described by the biomes (Fay and McKinley, 2014a) and basin boundaries.

References

Abernathey, R., Marshall, J. C., & Ferreira, D. (2011). The Dependence of Southern Ocean Meridional Overturning on Wind Stress. *Journal of Physical Oceanography*, *41*(12), 2261–2278. https://doi.org/10.1175/JPO-D-11-023.1

Arrigo, K. R., van Dijken, G. L., & Bushinsky, S. (2008). Primary production in the Southern Ocean, 1997-2006. *Journal of Geophysical Research*, *113*(8), 1997–2006. https://doi.org/10.1029/2007JC004551

Atlas, R., Hoffman, R. N., Ardizzone, J., Leidner, S. M., Jusem, J. C., Smith, D. K., & Gombos, D. (2011). A Cross-calibrated, Multiplatform Ocean Surface Wind Velocity Product for Meteorological and Oceanographic Applications. *Bulletin of the American Meteorological Society*, *92*(2), 157–174. https://doi.org/10.1175/2010BAMS2946.1

Bakker, D. C. E., Hoppema, M., Schr, M., Geibert, W., & Baar, H. J. W. De. (2008). A rapid transition from ice covered CO2-rich waters to a biologically mediated CO2 sink in the eastern Weddell Gyre. *Biogeosciences*, *5*, 1373–1386.

Bakker, D. C. E., Pfeil, B., Landa, C. S., Metzl, N., O'Brien, K. M., Olsen, A., … Xu, S. (2016). A multi-decade record of high-quality fCO2 data in version 3 of the Surface Ocean CO2 Atlas (SOCAT). *Earth System Science Data*, *8*(2), 383–413. https://doi.org/10.5194/essd-8-383-2016

Barnes, E. A., & Hartmann, D. L. (2010). Dynamical Feedbacks of the Southern Annular Mode in Winter and Summer. *Journal of the Atmospheric Sciences*, *67*(2007), 2320–2330. https://doi.org/10.1175/2010JAS3385.1

Boyd, P. W., & Ellwood, M. J. (2010). The biogeochemical cycle of iron in the ocean. *Nature Geoscience*, *3*(10), 675–682. https://doi.org/10.1038/ngeo964

~~Butterworth, B. J., & Miller, S. D. (2016). Air-sea exchange of carbon dioxide in the Southern Ocean and Antarctic marginal ice zone. *Geophysical Research Letters*, *43*(13), 7223–7230. https://doi.org/10.1002/2016GL069581~~

Carranza, M. M., & Gille, S. T. (2015). Southern Ocean wind-driven entrainment enhances satellite chlorophyll-a through the summer. *Journal of Geophysical Research: Oceans*, *120*(1), 304–323. https://doi.org/10.1002/2014JC010203

CDIAC. (2017). *Multi-laboratory compilation of atmospheric carbon dioxide data for the period 1957-2016*. NOAA Earth System Research Laboratory, Global Monitoring Division. https://doi.org/10.15138/G3CW4Q

de Boyer Montégut, C., Madec, G., Fischer, A. S., Lazar, A., & Iudicone, D. (2004). Mixed layer depth over the global ocean: An examination of profile data and a profile-based climatology. *Journal of Geophysical Research*, *109*(12), 1–20. https://doi.org/10.1029/2004JC002378

DeVries, T., Holzer, M., & Primeau, F. (2017). Recent increase in oceanic carbon uptake driven by weaker upper-ocean overturning. *Nature*, *542*(7640), 215–218. https://doi.org/10.1038/nature21068

du Plessis, M., Swart, S., Ansorge, I. J., ~~Dufour, C. O., Sommer, J. Le, Gehlen, M., Orr, J. C., Molines, J. M., Simeon, J., & Barnier, B. (2013). Eddy compensation and controls of the enhanced sea-to-air CO2 flux during positive phases of the Southern Annular Mode. *Global Biogeochemical Cycles*, *27*(3), 950–961. https://doi.org/10.1002/gbc.20090~~
& Mahadevan, A. (2017). Submesoscale processes promote seasonal restratification in the Subantarctic Ocean. *Journal of Geophysical Research*, *122*(4), 2960–2975. https://doi.org/10.1002/2016JC012494

Fay, A. R., & McKinley, G. A. (2014). Global open-ocean biomes: Mean and temporal variability. *Earth System Science Data*, *6*(2), 273–284. https://doi.org/10.5194/essd-6-273-2014

Fay, A. R., McKinley, G. A., & Lovenduski, N. S. (2014). Southern Ocean carbon trends: Sensitivity to methods. *Geophysical Research Letters*, *41*(19), 6833–6840. https://doi.org/10.1002/2014GL061324

Fogt, R. L., Jones, J. M., & Renwick, J. (2012). Seasonal zonal asymmetries in the southern annular mode and their impact on regional temperature anomalies. *Journal of Climate*, *25*(18), 6253–6270. https://doi.org/10.1175/JCLI-D-11-00474.1

Gade, K. (2010). A Non-singular Horizontal Position Representation. *Journal of Navigation*, *63*(3), 395–417. https://doi.org/10.1017/S0373463309990415

Gregor, L., Kok, S., & Monteiro, P. M. S. (2017). Empirical methods for the estimation of Southern Ocean CO2: support vector and random forest regression. *Biogeosciences*, *14*(23), 5551–5569. https://doi.org/10.5194/bg-14-5551-2017

Gurney, K. R., Law, R. M., Denning, A. S., Rayner, P. J., Pak, B. C., Baker, D., … Taguchi, S. (2004). Transcom 3 inversion intercomparison: Model mean results for the estimation of seasonal carbon sources and sinks. *Global Biogeochemical Cycles*, *18*(1), n/a-n/a. https://doi.org/10.1029/2003GB002111

Hauck, J., Völker, C., Wang, T., Hoppema, M., Losch, M., & Wolf-Gladrow, D. A. (2013). Seasonally different carbon flux changes in the Southern Ocean in response to the southern annular mode. *Global Biogeochemical Cycles*, *27*(4), 1236–1245. https://doi.org/10.1002/2013GB004600

Hoppema, M., Fahrbach, E., Stoll, M. H. C., & de Baar, H. J. W. (1999). Annual uptake of atmospheric CO2 by the Weddell sea derived from a surface layer balance, including estimations of entrainment and new production. *Journal of Marine Systems*, *19*(4), 219–233. https://doi.org/10.1016/S0924-7963(98)00091-8

~~Ishii, M., Inoue, H. Y., Matsueda, H., & Tanoue, E. (1998). Close coupling between seasonal biological production and dynamics of dissolved inorganic carbon in the Indian Ocean sector and the western Pacific Ocean sector of the Antarctic Ocean. *Deep-Sea Research Part I: Oceanographic Research Papers*, 45(7), 1187–1209. https://doi.org/10.1016/S0967-0637(98)00010-7~~

Jones, S. D., Le Quéré, C., & Rdenbeck, C. (2012). Autocorrelation characteristics of surface ocean $p\mathrm{CO_2}$ and air-sea CO2 fluxes. *Global Biogeochemical Cycles*, *26*(2), 1–12. https://doi.org/10.1029/2010GB004017

Kanamitsu, M., Ebisuzaki, W., Woollen, J., Yang, S. K., Hnilo, J. J., Fiorino, M., & Potter, G. L. (2002). NCEP-DOE AMIP-II reanalysis (R-2). *Bulletin of the American Meteorological Society*, *83*(11), 1631–1643+1559. https://doi.org/10.1175/BAMS-83-11-1631

Khatiwala, S., Tanhua, T., Mikaloff Fletcher, S. E., Gerber, M., Doney, S. C., Graven, H. D., … Sabine, C. L. (2013). Global ocean storage of anthropogenic carbon. *Biogeosciences*, *10*(4), 2169–2191. https://doi.org/10.5194/bg-10-2169-2013

Landschützer, P., Gruber, N., & Bakker, D. C. E. (2016). Decadal variations and trends of the global ocean carbon sink. *Global Biogeochemical Cycles*, *30*(10), 1396–1417. https://doi.org/10.1002/2015GB005359

Landschützer, P., Gruber, N., & Bakker, D. C. E. (2017). An updated observation-based global monthly gridded sea surface $p\mathrm{CO_2}$ and air-sea CO2 flux product from 1982 through 2015 and its monthly climatology (NCEI Accession 0160558) Version 2.2.

Landschützer, P., Gruber, N., Bakker, D. C. E., & Schuster, U. (2014). Recent variability of the global ocean carbon sink. *Global and Planetary Change*, 927–949. https://doi.org/10.1002/2014GB004853.Received

Landschützer, P., Gruber, N., Haumann, F. A., Rödenbeck, C., Bakker, D. C. E., Van Heuven, S. M. A. C., … Wanninkhof, R. H. (2015). The reinvigoration of the Southern Ocean carbon sink. *Science*, *349*(6253), 1221–1224. https://doi.org/10.1126/science.aab2620

Le Quéré, C., Rödenbeck, C., Buitenhuis, E. T., Conway, T. J., Langenfelds, R., Gomez, A., … Heimann, M. (2007). Saturation of the Southern Ocean CO2 Sink Due to Recent Climate Change. *Science*, *316*(5832), 1735–1738. https://doi.org/10.1126/science.1137004

Lenton, A., Codron, F., Bopp, L., Metzl, N., Cadule, P., Tagliabue, A., & Le Sommer, J. (2009). Stratospheric ozone depletion reduces ocean carbon uptake and enhances ocean acidification. *Geophysical Research Letters*, *36*(12), 1–5. https://doi.org/10.1029/2009GL038227

Lenton, A., & Matear, R. J. (2007). Role of the Southern Annular Mode (SAM) in Southern Ocean CO2 uptake. *Global Biogeochemical Cycles*, *21*(2), 1–17. https://doi.org/10.1029/2006GB002714

Lenton, A., Metzl, N., Takahashi, T. T., Kuchinke, M., Matear, R. J., Roy, T., … Tilbrook, B. (2012). The observed evolution of oceanic $p\mathrm{CO_2}$ and its drivers over the last two decades. *Global Biogeochemical Cycles*, *26*(2), 1–14. https://doi.org/10.1029/2011GB004095

Lenton, A., Tilbrook, B., Law, R. M., Bakker, D. C. E., Doney, S. C., Gruber, N., … Takahashi, T. T. (2013). Sea-air CO2 fluxes in the Southern Ocean for the period 1990-2009. *Biogeosciences*, *10*(6), 4037–4054. https://doi.org/10.5194/bg-10-4037-2013

Lévy, M., Iovino, D., Resplandy, L., Klein, P., Madec, G., Tréguier, A. M., … Takahashi, K. (2012). Large-scale impacts of submesoscale dynamics on phytoplankton: Local and remote effects. *Ocean Modelling*, *43–44*, 77–93. https://doi.org/10.1016/j.ocemod.2011.12.003

Lovenduski, N. S., Gruber, N., & Doney, S. C. (2008). Toward a mechanistic understanding of the decadal trends in the Southern Ocean carbon sink. *Global Biogeochemical Cycles*, *22*(3), 9. https://doi.org/10.1029/2007GB003139

Lovenduski, N. S., Gruber, N., Doney, S. C., & Lima, I. D. (2007). Enhanced CO2 outgassing in the Southern Ocean from a positive phase of the Southern Annular Mode. *Global Biogeochemical Cycles*, *21*(2), 1–14. https://doi.org/10.1029/2006GB002900

Mahadevan, A., D'Asaro, E., Lee, C., & Perry, M. J. (2012). Eddy-Driven Stratification Initiates North Atlantic Spring Phytoplankton Blooms. *Science*, *337*(6090), 54–58. https://doi.org/10.1126/science.1218740

Mahadevan, A., Tagliabue, A., Bopp, L., Lenton, A., Mémery, L., & Lévy, M. (2011). Impact of episodic vertical fluxes on sea surface $p\mathrm{CO_2}$. *Philosophical Transactions of the Royal Society*, *369*(1943), 2009–2025. https://doi.org/10.1098/rsta.2010.0340

Maritorena, S., & Siegel, D. A. (2005). Consistent merging of satellite ocean color data sets using a bio-optical model. *Remote Sensing of Environment*, *94*(4), 429–440. https://doi.org/10.1016/j.rse.2004.08.014

Marshall, G. J. (2003). Trends in the Southern Annular Mode from observations and reanalyses. *Journal of Climate*, *16*(24), 4134–4143. https://doi.org/10.1175/1520-0442(2003)016<4134:TITSAM>2.0.CO;2

McGillicuddy, D. J. (2016). *Mechanisms of Physical-Biological-Biogeochemical Interaction at the Oceanic Mesoscale*. *Annual Review of Marine Science* (Vol. 8). https://doi.org/10.1146/annurev-marine-010814-015606

McNeil, B. I., & Matear, R. J. (2013). The non-steady state oceanic CO2 signal: Its importance, magnitude and a novel way to detect it. *Biogeosciences*, *10*(4), 2219–2228. https://doi.org/10.5194/bg-10-2219-2013

Menemenlis, D., Campin, J., Heimbach, P., Hill, C. N., Lee, T., Nguyen, A., … J-M. Campin. (2008). ECCO2 : High Resolution Global Ocean and Sea Ice Data Synthesis. *Mercator Ocean Quarterly Newsletter*, *31*(October), 13–21. Retrieved from http://www.mercator-ocean.fr/content/download/691/5904/version/1/file/lettre_31_en.pdf#page=13

Meredith, M. P. (2016). Understanding the structure of changes in the Southern Ocean eddy field. *Geophysical Research Letters*, *43*(11), 5829–5832. https://doi.org/10.1002/2014JC010066.Received

Metzl, N., Brunet, C., Jabaud-Jan, A., Poisson, A., & Schauer, B. (2006). Summer and winter air-sea CO2 fluxes in the Southern Ocean. *Deep-Sea Research Part I: Oceanographic Research Papers*, *53*(9), 1548–1563. https://doi.org/10.1016/j.dsr.2006.07.006

Mongwe, N. P., Chang, N., & Monteiro, P. M. S. (2016). The seasonal cycle as a mode to diagnose biases in modelled CO 2 fluxes in the Southern Ocean. *Ocean Modelling*, *106*, 90–103. https://doi.org/10.1016/j.ocemod.2016.09.006

Monteiro, P. M. S., Gregor, L., Lévy, M., Maenner, S., Sabine, C. L., & Swart, S. (2015). Intraseasonal variability linked to sampling alias in air-sea CO2 fluxes in the Southern Ocean. *Geophysical Research Letters*, *42*(20), 8507–8514. https://doi.org/10.1002/2015GL066009

Munro, D. R., Lovenduski, N. S., Takahashi, T. T., Stephens, B. B., Newberger, T., & Sweeney, C. (2015). Recent evidence for a strengthening CO2 sink in the Southern Ocean from carbonate system measurements in the Drake Passage (2002-2015). *Geophysical Research Letters*, *42*(18), 7623–7630. https://doi.org/10.1002/2015GL065194

Nicholson, S. A., Lévy, M., Llort, J., Swart, S., & Monteiro, P. M. S. (2016). Investigation into the impact of storms on sustaining summer primary productivity in the Sub-Antarctic Ocean. *Geophysical Research Letters*, *43*(17), 9192–9199. https://doi.org/10.1002/2016GL069973

Pfeil, B., Olsen, A., Bakker, D. C. E., Hankin, S., Koyuk, H., Kozyr, A., … Yoshikawa-Inoue, H. (2013). A uniform, quality controlled Surface Ocean CO2 Atlas (SOCAT). *Earth System Science Data*, *5*(1), 125–143. https://doi.org/10.5194/essd-5-125-2013

Reynolds, R. W., Smith, T. M., Liu, C., Chelton, D. B., Casey, K. S., & Schlax, M. G. (2007). Daily high-resolution-blended analyses for sea surface temperature. *Journal of Climate*, *20*(22), 5473–5496. https://doi.org/10.1175/2007JCLI1824.1

Ritter, R., Landschützer, P., Gruber, N., Fay, A. R., Iida, Y., Jones, S., … Zeng, J. (2017). Observation-Based Trends of the Southern Ocean Carbon Sink. *Geophysical Research Letters*, *2*, 339–348. https://doi.org/10.1002/2017GL074837

Rödenbeck, C., Bakker, D. C. E., Gruber, N., Iida, Y., Jacobson, A. R., Jones, S. D., … Zeng, J. (2015). Data-based estimates of the ocean carbon sink variability - First results of the Surface Ocean pCO_2 Mapping intercomparison (SOCOM). *Biogeosciences*, *12*(23), 7251–7278. https://doi.org/10.5194/bg-12-7251-2015

Rödenbeck, C., Bakker, D. C. E., Metzl, N., Olsen, A., Sabine, C. L., Cassar, N., … Heimann, M. (2014). Interannual sea-air CO2 flux variability from an observation-driven ocean mixed-layer scheme. *Biogeosciences*, *11*(17), 4599–4613. https://doi.org/10.5194/bg-11-4599-2014

Rödenbeck, C., Keeling, R. F., Bakker, D. C. E., Metzl, N., Olsen, A., Sabine, C. L., & Heimann, M. (2013). Global surface-ocean pCO_2 and sea-Air CO2 flux variability from an observation-driven ocean mixed-layer scheme. *Ocean Science*, *9*(2), 193–216. https://doi.org/10.5194/os-9-193-2013

Rodgers, K. B., Aumont, O., Mikaloff Fletcher, S. E., Plancherel, Y., Bopp, L., de Boyer Montégut, C., … Wanninkhof, R. H. (2014). Strong sensitivity of Southern Ocean carbon uptake and nutrient cycling to wind stirring. *Biogeosciences*, *11*(15), 4077–4098. https://doi.org/10.5194/bg-11-4077-2014

Sabine, C. L., Hankin, S., Koyuk, H., Bakker, D. C. E., Pfeil, B., Olsen, A., … Yoshikawa-Inoue, H. (2013). Surface Ocean CO2 Atlas (SOCAT) gridded data products. *Earth System Science Data*, *5*(1), 145–153. https://doi.org/10.5194/essd-5-145-2013

Sallée, J.-B., Speer, K., & Rintoul, S. R. (2010). Zonally asymmetric response of the Southern Ocean mixed-layer depth to the Southern Annular Mode. *Nature Geoscience*, *3*(4), 273–279. https://doi.org/10.1038/ngeo812

Sasse, T. P., McNeil, B. I., & Abramowitz, G. (2013). A novel method for diagnosing seasonal to ~~inter-annual~~interannual surface ocean carbon dynamics from bottle data using neural networks. *Biogeosciences*, *10*(6), 4319–4340. https://doi.org/10.5194/bg-10-4319-2013

Shetye, S. S., Mohan, R., Patil, S., Jena, B., Chacko, R., George, J. V., … Sudhakar, M. (2015). Oceanic pCO_2 in the Indian sector of the Southern Ocean during the austral summer–winter transition phase. *Deep Sea Research Part II: Topical Studies in Oceanography*, *118*, 250–260. https://doi.org/10.1016/j.dsr2.2015.05.017

Swart, S., Speich, S., Ansorge, I. J., & Lutjeharms, J. R. E. (2010). An altimetry-based gravest empirical mode south of Africa: 1. Development and validation. Journal of Geophysical Research, 115(C3), 1–19. https://doi.org/10.1029/2009JC005299

Swart, N. C., & Fyfe, J. C. (2012). Observed and simulated changes in the Southern Hemisphere surface westerly wind-stress. *Geophysical Research Letters*, *39*(16), 6–11. https://doi.org/10.1029/2012GL052810

Swart, N. C., Fyfe, J. C., Gillett, N., & Marshall, G. J. (2015). Comparing trends in the southern annular mode and surface westerly jet. *Journal of Climate*, *28*(22), 8840–8859. ~~https://doi.org/10.1175/JCLI-D-15-0334.1~~https://doi.org/10.1175/JCLI-D-15-0334.1

~~Swart,~~ Swart, ~~S., Speich, S., Ansorge, I. J., & Lutjeharms, J. R. E. (2010). An altimetry-based gravest empirical mode south of Africa: 1. Development and validation. Journal of Geophysical Research, 115(C3), 1–19. https://doi.org/10.1029/2009JC005299~~

~~Swart,~~ S., Thomalla, S. J., & Monteiro, P. M. S. (2015). The seasonal cycle of mixed layer dynamics and phytoplankton biomass in the Sub-Antarctic Zone: A high-resolution glider experiment. *Journal of Marine Systems*, *147*, 103–115. https://doi.org/10.1016/j.jmarsys.2014.06.002

Tagliabue, A., ~~Bowie, A. R., Philip, W., Buck, K. N., Johnson, K. S., & Saito, M. A. (2017). The integral role of iron in ocean biogeochemistry. *Nature*, *543*(7643), In Press. https://doi.org/10.1038/nature21058~~
~~Tagliabue, A.,~~ Sallée, J.-B., Bowie, A. R., Lévy, M., Swart, S., & Boyd, P. W. (2014). Surface-water iron supplies in the Southern Ocean sustained by deep winter mixing. *Nature Geoscience*, *7*(March), 314–320. https://doi.org/10.1038/NGEO2101

Takahashi, T. T., Olafsson, J., Goddard, J. G., Chipman, D. W., & Sutherland, S. C. (1993). Seasonal variation of CO 2 and nutrients in the high-latitude surface oceans: A comparative study. *Global Biogeochemical Cycles*, *7*(4), 843–878. https://doi.org/10.1029/93GB02263

Takahashi, T. T., Sutherland, S. C., Sweeney, C., Poisson, A., Metzl, N., Tilbrook, B., … Nojiri, Y. (2002). Global sea-air CO2 flux based on climatological surface ocean $p\mathrm{CO_2}$, and seasonal biological and temperature effects. *Deep-Sea Research Part II: Topical Studies in Oceanography*, *49*(9–10), 1601–1622. https://doi.org/10.1016/S0967-0645(02)00003-6

Takahashi, T. T., Sutherland, S. C., Wanninkhof, R. H., Sweeney, C., Feely, R. A., Chipman, D. W., … de Baar, H. J. W. (2009). Climatological mean and decadal change in surface ocean $p\mathrm{CO_2}$, and net sea–air CO2 flux over the global oceans. *Deep-Sea Research Part II: Topical Studies in Oceanography*, *56*(8–10), 554–577. https://doi.org/10.1016/j.dsr2.2008.12.009

Thomalla, S. J., Fauchereau, N., Swart, S., & Monteiro, P. M. S. (2011). Regional scale characteristics of the seasonal cycle of chlorophyll in the Southern Ocean. *Biogeosciences*, *8*(10), 2849–2866. https://doi.org/10.5194/bg-8-2849-2011

Wang, S., & Moore, J. K. (2012). Variability of primary production and air-sea CO2 flux in the Southern Ocean. *Global Biogeochemical Cycles*, *26*(1), 1–12. https://doi.org/10.1029/2010GB003981

Wanninkhof, R. H., Asher, W. E., Ho, D. T., Sweeney, C., & McGillis, W. R. (2009). Advances in Quantifying Air-Sea Gas Exchange and Environmental Forcing*. *Annual Review of Marine Science*, *1*(1), 213–244. https://doi.org/10.1146/annurev.marine.010908.163742

Weiss, R. (1974). Carbon dioxide in water and seawater: the solubility of a non-ideal gas. *Marine Chemistry*, *2*(3), 203–215. https://doi.org/10.1016/0304-4203(74)90015-2

Wentz, F. J., Scott, J., Hoffman, R., Leidner, M., Atlas, R., & Ardizzone, J. (2015). Remote Sensing Systems Cross-Calibrated Multi-Platform (CCMP) 6-hourly ocean vector wind analysis product on 0.25 deg grid, Version 2.0. Retrieved March 5, 2017, from www.remss.com/measurements/ccmp

Whitt, D. B., Lévy, M., & Taylor, J. R. (2017). Low-frequency and high-frequency oscillatory winds synergistically enhance nutrient entrainment and phytoplankton at fronts. *Journal of Geophysical Research*, *122*(2), 1016–1041. https://doi.org/10.1002/2016JC012400